Spring 1-1-2016

On the Role of Cell Distribution in Hydrolytically Degradable Hydrogels for Tissue Engineering

Gaspard de Roucy
University of Colorado at Boulder, gaspard.deroucy@colorado.edu

On the role of cell distribution in hydrolytically degradable hydrogels for tissue engineering

by

Gaspard de Roucy

A thesis submitted to the

Faculty of the Graduate School of the

University of Colorado in partial fulfillment

of the requirements for the degree of

Master of Science

Department of Civil Engineering

2016

This thesis entitled:
On the role of cell distribution in hydrolytically degradable hydrogels for tissue engineering
written by Gaspard de Roucy
has been approved for the Department of Civil Engineering

_____

Prof. Franck Vernerey

_____

Prof. Stephanie Bryant

_____

Prof. Richard Regueiro

Date _____

The final copy of this thesis has been examined by the signatories, and we find that both the content and the form meet acceptable presentation standards of scholarly work in the above mentioned discipline.

de Roucy, Gaspard (MSc., Civil, Environmental and Architectural Engineering)

On the role of cell distribution in hydrolytically degradable hydrogels for tissue engineering

Thesis directed by Prof. Franck Vernerey

Degradable hydrogels have recently become prominent materials in the field of tissue engineering. They can be submitted to two degradation process: hydrolytic and enzymatic. For hydrolytically degradable systems, results seem to differ between samples. Yet the reasons for such a phenomenon have not been clearly understood. The objective of this thesis is to establish a multiscale model for such hydrogels. With the hypothesis that cross-linking density varies within a cell-seeded hydrogel, the present thesis aims to interpret experimental results to model and predict their behavior. First, a three-dimensional cell distribution is generated based on the analysis of experimental microscopy images. Then, a finite difference and a finite element analysis are set to reproduce the behavior of a degrading hydrogel in time at both microscale (cells are singled out) and macroscale (cells are not distinct, the distribution is defined by cell density) using hexahedron elements.

Contents

Chapter

1 Introduction **1**

2 Growth Model **5**

2.1 Macromer synthesis and chondrocyte encapsulation 5

2.2 Cross-link degradation and reverse gelation 6

2.3 Diffusion equations 10

2.4 Constitutive relations 11

3 Cell distribution analysis **17**

3.1 Cluster identification from microscopy 17

3.2 Random generation of 3D macroscopic systems 22

4 Results and Interpretations **27**

4.1 Influence of cell distribution on a microscopic system 27

4.2 Influence of a clustered distribution on a macroscopic system 30

4.3 Final results and effect of cluster parameters on mechanical properties 35

5 Conclusion **39**

Bibliography **42**

Appendix

A Cluster distribution parameters extracted from experimental image analysis **45**

B Equivalence between R_d and d parameter **49**

C Numerical values of the influence of cluster distribution parameters **50**

Tables

Table

2.1 Influence of macroscopic cell density on the initial modulus 7

A.1 Cell distribution parameter extracted from microscopy images 45

B.1 Values of d parameter for various combinations of R_d and microscopic cell densities . 49

C.1 Influence of cluster parameters on minimum modulus 51

C.2 Influence of cluster parameters on maximum modulus 51

Figures

Figure

1.1 Multiscale systems 3

2.1 Variation of initial cross-linking density around cells 8

2.2 Nodal displacements in the system after a ten percent axial compression 16

3.1 Cell distribution analysis : from microscopy images to numerical reproduction 19

3.2 Cell density mapping for cluster identification 21

3.3 Three dimensional generalization of cluster distribution 24

3.4 Influence of varying cluster parameters 26

4.1 Evolution of a microscopic system properties in time 28

4.2 Evolution of a macroscopic system properties in time 32

4.3 Identification of R_d for experimental results 32

4.4 Influence of d parameter on microscopic systems 34

4.5 Quantities used to evaluate the efficiency of a cell distribution 36

4.6 Influence of cluster distribution on mechanical performance 37

A.1 Microscopy images for a cell density of 50 million cells/mL 46

A.2 Microscopy images for a cell density of 100 million cells/mL 47

A.3 Microscopy images for a cell density of 150 million cells/mL 48

Chapter 1

Introduction

Biological tissues in the human body are prone to degrade during their lifetime as a result of phenomenons such as aging, injuries or degenerative diseases. This type of issue can lead to considerable disabilities and decrease one's life quality. Despite the capacity of modern medicine to provide a solution by replacing damaged tissues with artificial prosthesis, such an operation requires heavy surgery and long rehabilitation while not completely easing the discomfort for the patient. Therefore an efficient way to tackle this problem is found in tissue engineering. The objective of the procedure is to provide a cell-seeded scaffold by injecting a protective medium with encapsulated cells. The polymer scaffold plays an important role supporting physiological loads while the cartilage cells, or chondrocytes, secrete the extracellular matrix to synthesize new and functional tissue. For this application, hydrogels have proven to be promising alternatives. Really, they permit cell encapsulation [20] and their properties are easily controlled[26]. With a structure close to those of biological tissues [1], they represent a good candidate for tissue engineering applications.

In the case of cartilage tissue regeneration, chondrocytes are encapsulated in a cross-linked polymer scaffold. They synthesize an extracellular matrix (ECM) which diffuses through the gel and deposits as a solid phase [6][10]. The newly deposited ECM constitutes the functional cartilage tissue. Despite their encouraging properties, hydrogels are limited by the tight polymer network necessary to achieve a high load-bearing capacity. Due to the size of ECM molecules, a decrease in cross-linking density is necessary to allow their diffusion [20][3]. Therefore cross-links are made sensitive to hydrolysis by the solvent to allow a degradation of the gel. The hydrolytic degradation

process allows tissue growth but also leads to a decrease in the load-bearing capacity of the system and endangers its susainability. In order to ensure successful tissue growth, it is necessary to analyze the behavior of a cell-seeded hydrogel in time. Consequently, there is a need for models conducting an analysis of favorable conditions and design parameters for effective hydrogels [13]. The necessary condition for system efficiency is to balance the degradation of cross-links with the growth of new tissue [12][14], to minimize the decreasing tendency of the modulus before the new deposited ECM can successfully resist external loads.

The systems studied in this thesis, illustrated in figure 1.1, consist of a mixture of cells and hydrogel. At the microscopic scale, the cells are distinct and their boundaries are well defined and observable. At the macroscopic scale, cells are too small to be singled out but their distribution is given by the local cell density. When a hydrogel is subject to hydrolytic degradation only, the cross-linking density decreases homogeneously everywhere in the medium. If the gel completely degrades before the new ECM molecules produced by cells can connect with each other, the new tissue will not be strong enough to ensure the mechanical integrity of the system. This leads to the assumption that cell distribution might be a deciding condition in the case of hydrolytically degradable hydrogels, by influencing the connectivity of deposited ECM. Therefore systems of various cell distributions must be analyzed. In these configurations, a macroscopic cell density will be fixed but their distribution will be heterogeneous within the gel, resulting in regions of low or high cell density at the micro-scale. With such a configuration, a hydrogel must be analyzed at two distinct scales: micro-structure (mechanical properties of the gel in a cell cluster or a low cell density volume) and macro-structure, which consists of a full sample with a fixed average cell density. The main objective of this thesis is to find potential parameters describing the influence of cell distribution from a fine analysis of experimental results. Therefore it would be interesting to come up with a model that could describe the key parameters of cell distribution at both scales. However, the objective of the model is not only to study connectivity, but to compute the mechanical properties of the gel at every step of the degradation process. This way, ECM connectivity and compressive modulus can be related, resulting in a quantitative description of gel sustainability

Figure 1.1: Microscale: cells are clearly distinct in the gel and their geometry must be taken into account in the model.
Macroscale: Cells are too small compared to the volume of gel considered in the system to be singled out. Their distribution is represented by mapping the local cell density at every material point

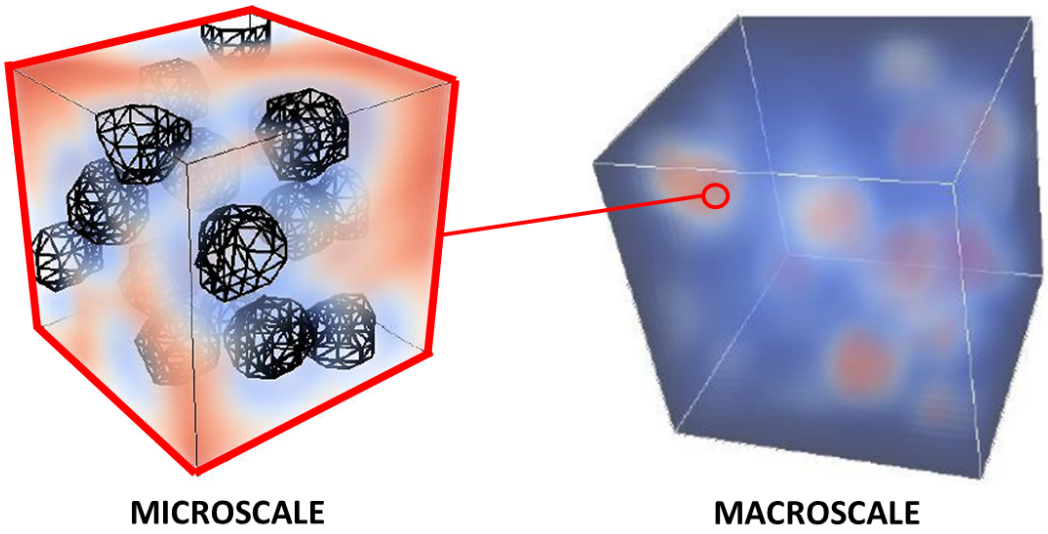

instead of an "all or nothing" behavior which only depends on connectivity.

A limitation for the model resides in the fact that hydrolytic degradation is a global process, bringing the entire gel to dissolve due to a lack of cross-links. This behavior is called reverse gelation. As a consequence, the entire medium has to collapse before allowing tissue growth, which does not allow tissue growth within the scaffold. Nevertheless, even for non-degradable hydrogels, experimental data shows a diffusion of ECM in the near-surroundings of chondrocytes. Additionally, an increase of cell density significantly lowers the initial modulus of a cell-seeded hydrogel. Such observations lead to making the assertion that cells have an influence on polymerization, and decrease the cross-linking density in their nearby region. Following this assumption, connectivity is expected to happen faster for regions of high cell density, since ECM diffusion and deposition are supposed to be allowed at early time steps, before the polymer network loses its mechanical integrity. Consequently, a second hypothesis can be made: cell distribution influences the result of tissue regeneration in hydrolytically degradable hydrogels. This aspect presents an interest to the field of tissue engineering since previous studies have focused on the cell environment (scaffold composition, nutrients present in the gel, enzymatic degradation...) but have very often supposed a homogeneous distribution of cells and focused on the micro-scale.

In the first section, the present thesis focuses on the processes of degradation, diffusion and deposition. Their implementation in the model are described and the hypothesis concerning the influence of cells on polymerization is illustrated and quantified. An influence parameter will be introduced to characterize the importance of the influence. The framework for the finite element mechanical analysis is also explained. Then, section 3 tackles the issue of the cell distribution analysis. Clustered cell distributions are defined, and their identification in experimental results is clarified. Finally, the last section is built around the analysis and discussion around the results obtained for microscopic and macroscopic results. The link between both scales is also described to clarify the homogenization process necessary to evaluate mechanical properties at the macro-scale.

Chapter 2

Growth Model

Cartilage tissue growth mechanism consists in a deposition of new extracellular matrix (ECM) produced by the chondrocytes. However it is not strong enough to support any external loading during its production. Hydrogels in tissue engineering act as scaffolds to support mechanical loads while the extracellular matrix is produced by cells, diffusing and depositing to form new tissue. However the hydrogel mesh size is usually too small compared to the size of ECM molecules to allow their diffusion. That is to say that the pores of the polymer network are too narrow to allow the diffusion of ECM molecules. Therefore the production of new tissue is limited to the direct surroundings of cells, and does not lead to satisfying results. As a consequence, it is necessary to introduce a degradation process to the polymer network which, by cleaving cross-links and enlarging the pores of the hydrogel, results in a larger mesh size. Then, ECM molecules are able to diffuse through the hydrogel. The issue is that while the gel degrades, its load-bearing capacities decrease as well, until only the solvent and soluble polymer chains resulting from degradation remain. In this model, we focus on bulk degradation following a generic base catalyzed ester hydrolysis for a pH of 7.4 in the media, and make a hypothesis on the variation of polymer cross-linking density around cells.

2.1 Macromer synthesis and chondrocyte encapsulation

Before analyzing the repartition of a cell-seeded hydrogel, it is important to remind the experimental process behind their formation. The entirety of the experimental work on which this

thesis is based was conducted by Dr. Stephanie Bryant's group from the Chemical and Biological Efgineering department at the University of Colorado. The macromers of 8-arm PEG-caprolactone functionalized with norbornene were synthesized in a two step process unsing protocols adapted from Bryant, et al. Briefly, 8-arm PEG-hexaglycerol (20 kDa, JenKem Technology, Allen, TX) was reacted with 1.5 molar excess -caprolactone using tin(II) ethylhexanoate as the ring opening catalyst. The reaction was carried out at 140C for 6 h under vacuum. The intermediate product PEG8arm-CAP was recovered by precipitation in ice-cold diethyl ether. PEG8arm -CAP was reacted overnight at room temperature under argon with N,N-diisopropylcarbodiimide (10 molar excess), 4-dimethylaminopyridine (1 molar excess), pyridine (10 molar excess) and 5-norbornene-2-carboxylic acid (10 molar excess) ifn dichloromethane. The final product, PEG8arm -CAP-NB, was purified through filtration over activated carbon and precipitated in diethyl ether. The precipitate was dried and dissolved in a minimal amount of chloroform. The solution was washed twice in a glycine buffer (0.05 M NaCl, 0.05 M NaOH, and 0.05 M glycine) and once in a brine solution. The purified product was recovered via precipitation in diethyl ether, lyophilized, and confirmed by 1H nuclear magnetic resonance spectroscopy. The number of caprolactones per PEG arm was determined to be 1.26 by comparing the peak area for the methylene protons in the caprolactone (= 2.25-2.4 ppm) to the peak area of the methylene protons in PEG (= 3.25-3.9 ppm). Norbornene conjugation was determined to be 64.5

2.2 Cross-link degradation and reverse gelation

Experimental results from viability images and mechanical tests have shown a quick deposition of ECM in the close periphery of the cells in most cases. Additionally, the initial modulus of the hydrogel greatly decreases when the cell density increases as shown in table 2.1. It could be assumed that since chondrocytes represent soft insertions in the gel, the apparent decrease in modulus is only caused by their mechanical properties. However early simulations from the model considering a homogeneous gel with soft inclusions as cells did not match such an important drop in initial modulus. These results suggest that the presence of cells in the gel influences the poly-

Table 2.1: Influence of macroscopic cell density on the initial modulus

0 mill/mL	50 mill/mL	100 mill/mL	150 mill/mL
46.5 kPa	23.3 kPa	13.6 kPa	8.5 kPa

merization reaction, leading to an uneven cross-linking density in the initial system.

The cell influence is implemented in the model by using areas of lower initial cross-linking density ρ_x^0. Since the chondrocytes are not connected to the hydrogel, the initial cross-linking density is considered to be null on their boundaries. Then, a realistic function must be built to establish the evolution of the cross-linking density between cell boundary and the bulk of the gel. Experiments show that cells seem to attract and consume some of the free chains during polymerization, therefore a diffusion profile would be the most accurate to model this phenomenon. As a consequence, the evolution of the cross-linking density profile around a chondrocyte is computed using the following equation, and illustrated in figure 2.1:

$$\rho_x(X) = \rho_x^0(1 - \exp(-\frac{X - R}{l})) \tag{2.1}$$

$$l = \frac{R - R_d}{\ln(0.01)} \tag{2.2}$$

where X is the distance from the cell, R is the cell radius, R_d is the influence radius of the cell. The influence radius of a cell is defined as the distance between the center of a cell and the bulk of the gel. That is to say that around each chondrocyte, the initial cross-linking density varies as described in equation (2.1) in a sphere of radius R_d, and that $\rho_x(R_d) = \rho_x^0$. It is expressed in the model as a multiple of the cell radius. Additionaly, l is a length quantity found by matching $\rho_x(X = R_d)$ with 99% of ρ_x^0, hence the logarithmic term in its definition.

The influence radius parameter aims to quantify the influence of cells on polymerization and therefore the initial cross-linking density profile. It will possibly be a key parameter in the model,

Figure 2.1: The equation used to describe the cros-slinking density as a function of the distance from the cell is illustrated on the left graph. Illustrations aim to highlight the interpretation of the R_d influence parameter in a three dimensional system.

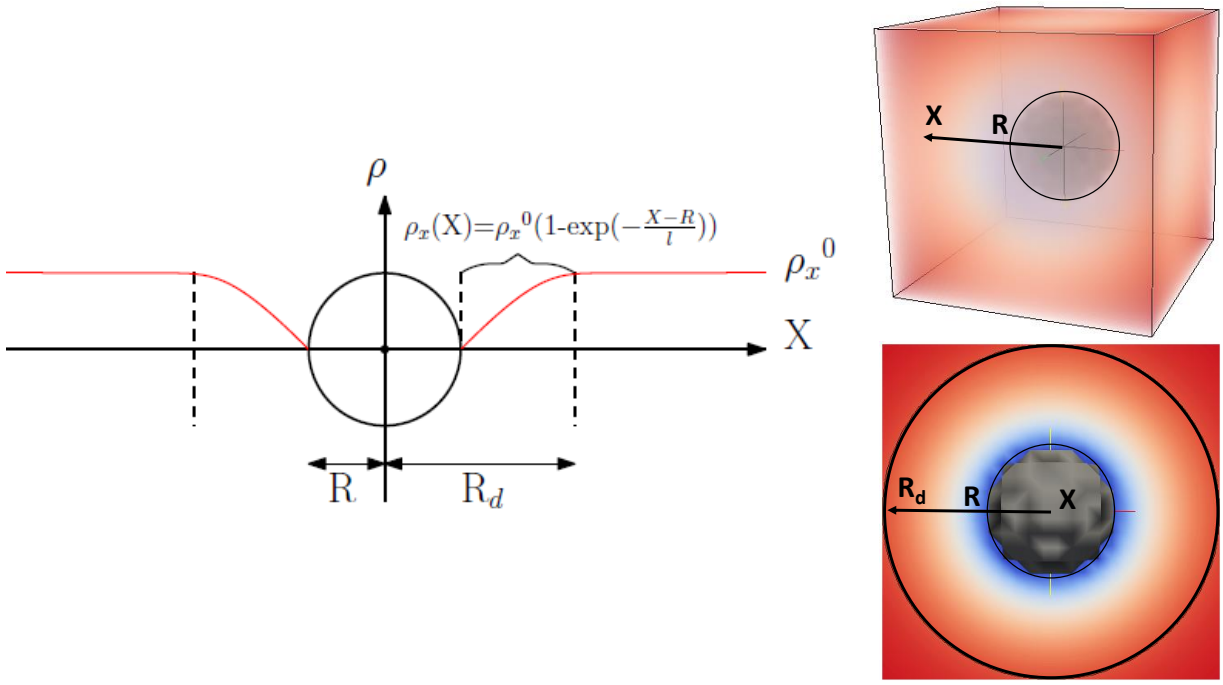

since it is fundamental to our first hypothesis. With the definition of the cell influence parameter R_d on the initial cross-linking density and its role in the model defined, the degradation process is still to be implemented. For tissue engineering application, a hydrogel must be designed to act as a scaffold for the chondrocytes while they synthesize ECM and before the growth mechanism has achieved sustainable mechanical properties. Consequently, it must have a satisfying load-bearing capacity. Since the stiffness of a hydrogel is strongly related to its cross-linking density, the mesh of the polymer network must be tight enough. As a result, its mesh size is too thin to allow the diffusion of extracellular matrix and the production of new tissue is compromised.

To overcome this problem, hydrogels are designed with degradable cross-links. The degradation process is made possible by synthesizing a gel which cross-links are sensitive to hydrolysis. Cross-links will react with the solvent and be cleaved, leading to a progressive and homogeneous decrease of cross-linking density in time for the bulk of the gel. Resulting from hydrolytic degradation, the mesh size of the polymer network increases as cross-links are cleaved, allowing diffusion and deposition of new ECM in the gel. For the degradation process, first order kinetics reactions are considered[18] where the cross-linking density in time follows the equation:

$$\begin{cases} \dfrac{D\rho_x}{Dt} = -k\rho_x \\ \\ \rho_x(\underline{\mathrm{x}}, 0) = \rho_x^0 \end{cases} \tag{2.3}$$

where k is the constant degradation rate. Therefore, the following function gives the evolution of the cross-linking density in time:

$$\rho_x(\underline{\mathrm{x}}, t) = \rho_x^0(\underline{\mathrm{x}})e^{-kt} \tag{2.4}$$

Following this equation, ρ_x decreases in time until it reaches a critical value, at which a minority of regions in the gel are still cross-linked but the connectivity between each of them is not ensured

anymore. At this point the last branches of the hydrogel dissolve and its mass is lost[20], as is its mechanical integrity. This phenomenon is called reverse gelation, and must be part of the model for the diffusion study in order to capture the real behavior of a degrading system. The model considers ECM molecules to be too large to diffuse before the gel in their surrounding area reaches reverse gelation.

2.3 Diffusion equations

Once the hydrolytic degradation of cross-links is implemented, on the second main process of tissue growth must be set: the diffusion and deposition of ECM particles in the hydrogel. In the model, cells are considered as constant sources of extracellular matrix. Since it is assumed that cross-linking density decreases around cells, reverse gelation will be reached faster in such regions. Therefore the diffusion of ECM is made possible at early times, leading to the synthesis of new tissue before the complete loss of load-bearing capacity in the bulk of the gel.

To implement this phenomenon, a finite difference approach must be used. That is to say the considered space is discretized in a given number of material points. Every point is attributed with an initial cross-link density and an initial concentration of ECM. Then, at each time step, a diffusion equation following Fick's laws is solved to evaluate the quantity of ECM diffusing from one point to its direct neighbors. This equation is ruled by one main diffusion coefficient D^*. However, as long as the cross-linking density is high, the ECM molecules are too big too diffuse and deposit, therefore a critical cross-linking density $\rho_{x,crit}$ is set, corresponding to the level at which reverse gelation is reached. As long as ρ_x is greater than $\rho_{x,crit}$, the diffusion coefficient D^* is null. We solve this problem at different areas of our entire volume. We use the following diffusion equation:

$$\begin{cases} \frac{\partial C}{\partial t} = D\nabla^2 C - \gamma C \\ C(\underline{\mathrm{x}}_{gel}, 0) = 0 \\ C(\underline{\mathrm{x}}_{cell}, 0) = 1 \\ C(\underline{\mathrm{x}}_{cell}, t) = 1 \end{cases} \tag{2.5}$$

where $\underline{x}_{gel}$ are the points of the gel distinct from cells, $\underline{x}_{cell}$ are the cell boundaries, C is the ECM concentration, γ is the deposition rate of fluid ECM turning into a solid phase C^*, and D is the diffusivity, which depends on the cross-linking density:

$$\begin{cases} D = 0 \quad if \quad \rho_x < \rho_{x,crit} \\ \\ D = D^* \quad if \quad \rho_x > \rho_{x,crit} \end{cases} \tag{2.6}$$

Therefore at each time step, the ECM concentration increases in regions reached by reverse gelation; however the fluid ECM diffusing in these free regions does not form a solid cartilage tissue with mechanical integrity. Before becoming a solid phase with its own mechanical properties, it deposits in the gel, with a constant deposition rate γ. To ensure the stability condition in the finite difference analysis, the length of a time step Δt is set as:

$$\Delta t = \frac{1}{6} \frac{\Delta x^2}{D^*} \tag{2.7}$$

By the end of this process, the model can run several simulations in a short amount of time to compute the time evolution of cross-linking density, ECM diffusion and tissue growth for different systems. However the composition of the gel is not sufficient to estimate its load-bearing capacity, and the mechanical analysis is a necessary step to complete the model.

2.4 Constitutive relations

Then a mechanical analysis of the system must be conducted to compute its macroscopic properties. To keep the computations as simple as possible, a linear, static finite element analysis is implemented. At every time step, the composition of the system is extracted from the diffusion problem results, and only the solid phase is considered. Supposing that the gel has linear elastic

properties [19], a planar compression is applied in a given direction and resulting stresses in the hydrogel are computed, to finally average the results over the macroscopic system.

To agree with the assumptions made for the model, it is important to remain in the linear elastic range of deformations. For biological tissues, a ten percent compression seems to be a reasonable choice to stay in the range of small strains [23] and ensure the validity of the method. The axial strain $\bar{\lambda}$ is applied in uniaxial stress condition, which leads to a stretch of $\frac{1}{\sqrt{\bar{\lambda}}}$ in the two other directions according to the incompressibility conditions. The resulting deformation gradient $\underline{\mathrm{F}}$ is:

$$\underline{\mathrm{F}} = \begin{pmatrix} \bar{\lambda} & 0 & 0 \\ 0 & \frac{1}{\sqrt{\bar{\lambda}}} & 0 \\ 0 & 0 & \frac{1}{\sqrt{\bar{\lambda}}} \end{pmatrix} \tag{2.8}$$

Now, we have to solve for the following equations with Dirichlet boundary conditions:

$$\begin{cases} \epsilon_{ij} = \frac{1}{2}(\frac{\mathbf{u}_i}{\partial \mathbf{x}_j} + \frac{\partial \mathbf{u}_j}{\partial \mathbf{x}_i}) \\ \sigma_{ij} = \mathbf{C}_{ijkl}\epsilon_{kl} \quad ; \quad \mathbf{C}_{ijkl} = \lambda\delta_{ij}\delta_{kl} + \mu(\delta_{ik}\delta_{jl} + \delta_{il}\delta_{jk}) \\ \frac{\partial \sigma_{ij}}{\partial \mathbf{x}_i} + \mathbf{b}_j = 0 \end{cases} \tag{2.9}$$

$$\begin{cases} \mathbf{u_x}(x=0) = 0 \quad ; \quad \mathbf{u_x}(x=L) = (\bar{\lambda} - 1)L \\ \mathbf{u_y}(y=0) = 0 \quad ; \quad \mathbf{u_y}(y=L) = (\frac{1}{\sqrt{\bar{\lambda}}} - 1)L \\ \mathbf{u_z}(z=0) = 0 \quad ; \quad \mathbf{u_z}(z=L) = (\frac{1}{\sqrt{\bar{\lambda}}} - 1)L \end{cases} \tag{2.10}$$

where λ and μ are the Lame constants, and $\mathbf{b}$ is the body force vector caused by the deformation. Then, after introducing a test function v which must be null on the boundaries, the principle of virtual work states that:

$$\int_\Omega \sigma_{ij}\, \delta\epsilon_{ij}\, d\Omega \, - \, \int_\Omega \mathbf{b}_i\, \delta v_i\, d\Omega \, = \, 0 \tag{2.11}$$

which gives:

$$\int_{\Omega} \mathbf{C}_{ijkl} \, \frac{\mathbf{u}_k}{\partial \mathbf{x}_l} \, \frac{\partial \delta \mathbf{v}_i}{\partial \mathbf{x}_j} \, d\Omega \; - \; \int_{\Omega} \mathbf{b}_i \, \delta v_i \, d\Omega \; = \; 0 \tag{2.12}$$

A linear finite element analysis is implemented using 8-node hexahedral elements. At each node i, the shape functions are defined as:

$$N_i = \frac{1}{8}(1 + \xi \, \xi_i)(1 + \eta \, \eta_i)(1 + \mu \, \mu_i) \tag{2.13}$$

Using the shape functions, the jacobian and strain-displacement matrices $\underline{\mathrm{J}}$ and $\underline{\mathrm{B}}$ can be calculated:

$$\underline{\mathrm{J}} = \begin{pmatrix} x_i \frac{\partial N_i}{\partial \xi} & y_i \frac{\partial N_i}{\partial \xi} & z_i \frac{\partial N_i}{\partial \xi} \\ x_i \frac{\partial N_i}{\partial \eta} & y_i \frac{\partial N_i}{\partial \eta} & z_i \frac{\partial N_i}{\partial \eta} \\ x_i \frac{\partial N_i}{\partial \mu} & y_i \frac{\partial N_i}{\partial \mu} & z_i \frac{\partial N_i}{\partial \mu} \end{pmatrix} \tag{2.14}$$

$$\underline{\mathrm{B}} = \begin{pmatrix} \frac{\partial N}{\partial x} & 0 & 0 \\ 0 & \frac{\partial N}{\partial y} & 0 \\ 0 & 0 & \frac{\partial N}{\partial z} \\ \frac{\partial N}{\partial y} & \frac{\partial N}{\partial x} & 0 \\ 0 & \frac{\partial N}{\partial z} & \frac{\partial N}{\partial y} \\ \frac{\partial N}{\partial z} & 0 & \frac{\partial N}{\partial x} \end{pmatrix} \tag{2.15}$$

Then, the element stiffness matrix $\underline{\mathrm{K}}^{(e)}$ is obtained by integrating:

$$\underline{\mathrm{K}}^{(e)} = \int_{-1}^{1} \int_{-1}^{1} \int_{-1}^{1} \underline{\mathrm{B}}^T \, \underline{\mathrm{C}}^{(e)} \, \underline{\mathrm{B}} \det(\underline{\mathrm{J}}) \, d\xi \, d\eta \, d\mu \tag{2.16}$$

which, by using a Gaussian quadrature with 2x2x2 integration points, can be estimated as:

$$\underline{\mathrm{K}}^{(e)} = \sum_{i=1}^{p} \sum_{i=1}^{p} \sum_{i=1}^{p} \underline{\mathrm{B}}_{ijk}^T \, \underline{\mathrm{C}}^{(e)} \, \underline{\mathrm{B}}_{ijk} \det(\underline{\mathrm{J}}_{ijk}) \, w_i \, w_j \, w_k \tag{2.17}$$

where p is the number of Gauss points in a given direction (p=2 in this case), w are the Gauss weights, and $\underline{\underline{\mathrm{C}}}^{(e)}$ is the element stress-strain matrix. For every element, $\underline{\underline{\mathrm{C}}}^{(e)}$ depends on the cross-linking density and deposited ECM concentration at the time of the computation. To obtain the stiffness of the polymer network, the modulus of every material point must be computed as a function of the cross-linking density ρ_x with an expression coming from the elastic energy of a gel:

$$G = \frac{\rho_x RT}{\nu_p} \tag{2.18}$$

$$E = 2G(1+\nu) \tag{2.19}$$

where G is the shear modulus, E is the Young's modulus, R is the gas constant, T is the temperature, ν_p is the molar volume of polymer, and ν is the Poisson's ratio. According to experimental results, cells have a Young's modulus of 1kPa [9]. However, an equation defining the stiffness of a solid ECM phase have not been defined yet. Therefore it will be computed as a linear function of the deposited ECM concentration C^*. The coefficient of this function will be a parameter of the model, set later to approach experimental values to estimate the ECM stiffness.

After assembling the global stiffness matrix with the components from every element, we can compute the displacement vector $\underline{\mathrm{u}}$ by solving:

$$\underline{\mathrm{u}} = \underline{\mathrm{K}}^{-1}\,\underline{\mathrm{f}} \tag{2.20}$$

This finite element analysis will be used twice in the process. First at the microscopic scale, it is necessary to obtain the Young's modulus of a material point for a given cell density. To do so, the previous analysis is applied to systems with a given cell density f and influence radius R_d. Then, E can be mapped as a function of these two parameters. At the macroscopic scale, the mapping from the previous step will be used to give each material point its corresponding stiffness and compute the overall modulus of the gel to get its mechanical properties at the macro-scale.

For the finite element analysis, an optimal mesh (number of elements in each direction) must be found to optimize the accuracy of the results and the computational cost of each simulation. To do so, several simulations were ran for a simple system, varying the number of elements for each simulation. They showed that a mesh of 15x15x15 elements leads to accurate results while keeping an acceptable computational cost at the microscopic scale. As a result, such systems seem optimal and the mesh can be set for the model.

Results of this analysis are illustrated further in chapter 4 at both scales. Figure 2.2 here presents a direct exemple of application of the displacement computations implemented in the model. the figure illustrates the material points in their initial coordinates and the displacements caused by the axial compression and incompressibility condition. For clarity purposes, the mesh size used in this example is coarse but the ones used in the model are refined as stated in the prevous paragraph.

Figure 2.2: Nodal displacements in the system after a ten percent axial compression

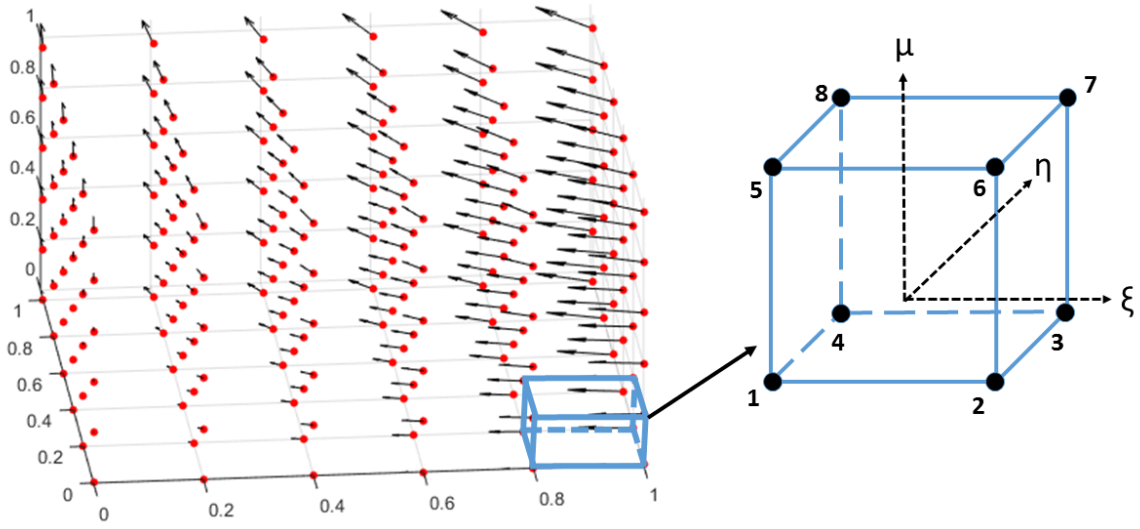

Chapter 3

Cell distribution analysis

The main objective of this model is to find what the optimal conditions on cell distribution and R_d parameter would be for a hydrolytically degradable hydrogel in order to obtain satisfying tissue growth. Initially, hydrogels with a homogeneous cell distribution might seem to be the best starting point. However according to the main hypothesis of the model, the influence of cells on polymerization would be much more efficient if combined with a clustered system in order to provide tissue connectivity at early times of the degradation process. To analyze this phenomenon, the model must include a random generation of macroscopic cell distributions which will be based on experimental results. Therefore realistic systems will be reproduced to evaluate the influence of the model parameters. Then, user defined cell distributions will be implemented to study the influence of clusters on tissue growth.

3.1 Cluster identification from microscopy

After obtaining samples of experimental images for viability results at day zero, the distribution of cells right after polymerization can be analyzed. It is easily noticeable that cells are not homogeneously distributed, and are gathered in small, close-range groups that we will define as clusters. To reproduce realistic results, the cluster distribution must be analyzed in details. The study will be performed for three different macroscopic cell densities (50, 100 and 150 million cells per mL). For each of them, five samples will be analyzed to account for the fact that cell distribution is not uniform at the macroscopic scale. The results will then be averaged to get cluster

parameters corresponding to a given density.

The first step to initiate the cluster analysis is to translate the experimental images to numerical data which will be usable to determine the parameters ruling the cell distribution. An automatic routine was written, which automatically loads any sample image to return its distribution properties. As shown in figure 3.1(a), this process follows multiple steps using the image processing toolbox from Matlab. First, the color composition of every pixel in the image is extracted and all non-green components are filtered (dead cells and part of the background noise). Then, every remaining green pixel is set at the same level in order to convert the image into a binary file. Binary images can be analyzed using the image analysis tools, however it still need a few last corrections before running the final analysis. Since some regions of the sample are highly populated, several groups of cells are seen as single large elements instead of distinct cells. To segment such regions and separate the cells when possible, a watershed transform is applied, which identifies the circular shapes and sets them as single cells. Finally the analysis can be conducted, to identify every element of the binary image and return an array giving their respective centroid coordinates and area. Nevertheless, it appears in figure 3.1(b) that some regions have not been segemented enough. To tackle this issue, a post-processing subroutine was built. First, the average cell area is computed for the sample. Then, the area of every element in the sample is compared to this average value, and divided in the corresponding number of cells if the area is too large. Once the image analysis is complete, a numerical reproduction of any microscopy sample can be produced automatically, in order to determine its distribution parameters.

Once the numerical data corresponding to every sample is available, it can be used to conduct the cluster analysis. This analysis is a keystone to produce conclusive results. Really, according to the initial hypothesis cell distribution might have a considerable influence on tissue growth in hydrolytically degradable gels. However being able to numerically reproduce experimental samples is not enough to model a wide range of cell distributions and study their influence. The following steps of the model aim to determine clear parameters ruling cell and cluster distribution in order to generate as many as needed. But first, the notion of cell cluster must be defined. Clusters are

Figure 3.1: Cell distribution analysis : from histology to numerical reproduction
(a) Experimental samples were converted to binary images after filtering the background noise to retrieve the coordinates and area of every cell
(b) Identification and segmentation of high cell density regions

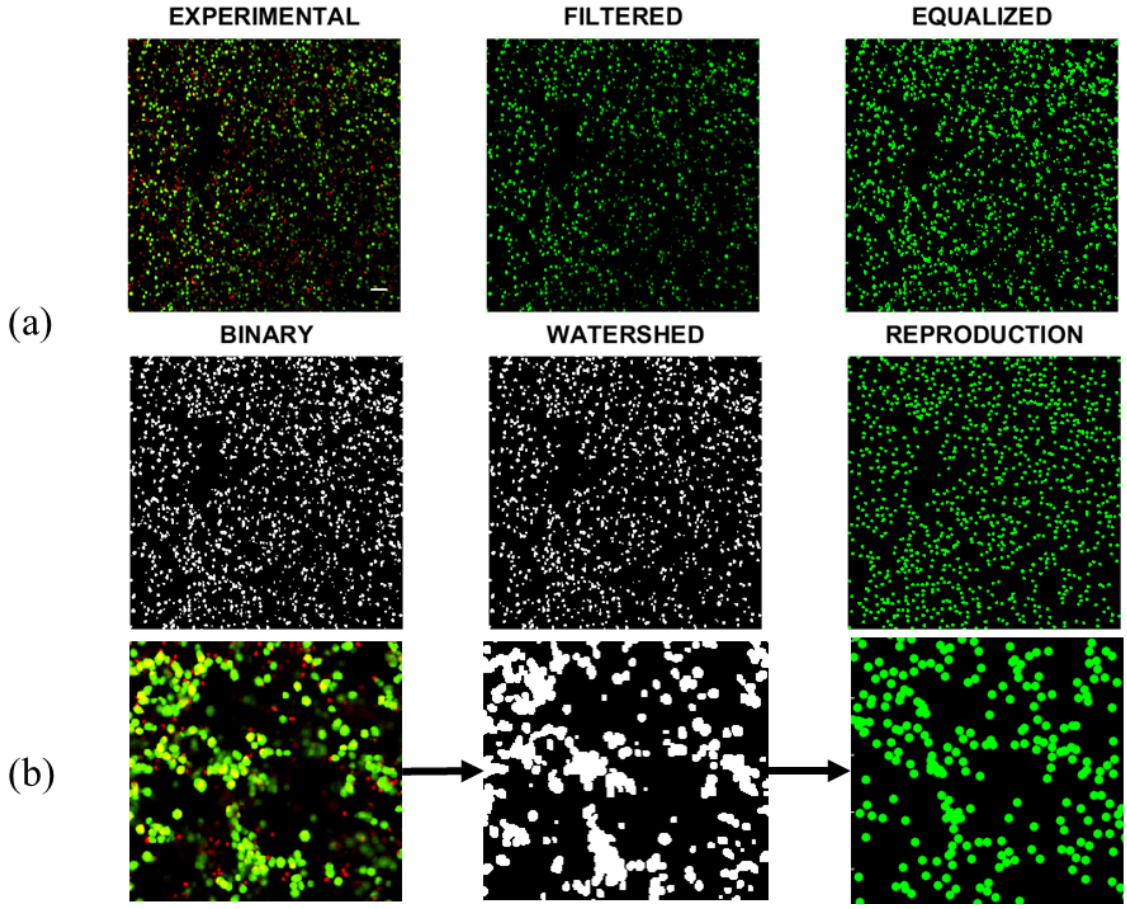

tight group of cells within a certain distance of each other. They will be identified as the regions of high cell density in the sample. In order to single them out and have better quantitative data to analyze the cell distribution, results from the image processing are used to map the cell density throughout the sample. To do so, the numerical representation of the cell distribution is finely meshed, and the local cell density is evaluated at every material point as illustrated in figure 3.2.

It is now possible to use the cell density mapping, to quantitatively estimate the cell distribution within the sample. To simplify the model, and ease the implementation of randomly generated systems, clusters are estimated as spherical multivariate normal distributions of cells. First, it is necessary to estimate the quantity of clusters by locating their center, and compute the average spacing between clusters. To do so, the previous results on cell density were processed to determine the location of local maxima in the sample, which are assumed to be cluster centers. Then, the average cluster spacing is assessed by identifying the average minimal distances between each cluster and its closest neighbors; and computing their mean.

Every cluster present in the sample was isolated as shown in figure 3.2. In a first iteration, the cluster is considered to have a radius equal to the average cluster spacing. Using this estimate, its cell population is identified, and the maximum density, covariance matrix and cluster radius are evaluated. These computations are then reiterated with the refined radius to obtain the final parameters for the bivariate cell distribution within a given cluster. By repeating these computations for every cluster, it is also possible to compute the total number of cells included in clusters, and the background noise of the distribution, which corresponds to single cells, located in low density regions.

Finally, by averaging the results over all samples, the cluster analysis routine returns an array of results containing, for all macroscopic cell densities: the total number of cells, total number of clusters, average spacing between clusters, average cluster radius, cluster covariance matrix with its eigenvalues, average peak cell density within clusters, and average background noise. For the range of samples currently available, the results are presented in appendix A. Such parameters define precisely the overall cell distribution within a sample, at the macroscopic scale and microscopic

Figure 3.2: Cell density mapping for cluster identification - Cell density is computed at every material point of the sample, and clusters, defined as the most populated regions, are identified at local maxima (black dots). Then, every cluster is isolated to identify its population and match a bivariatel normal distribution.

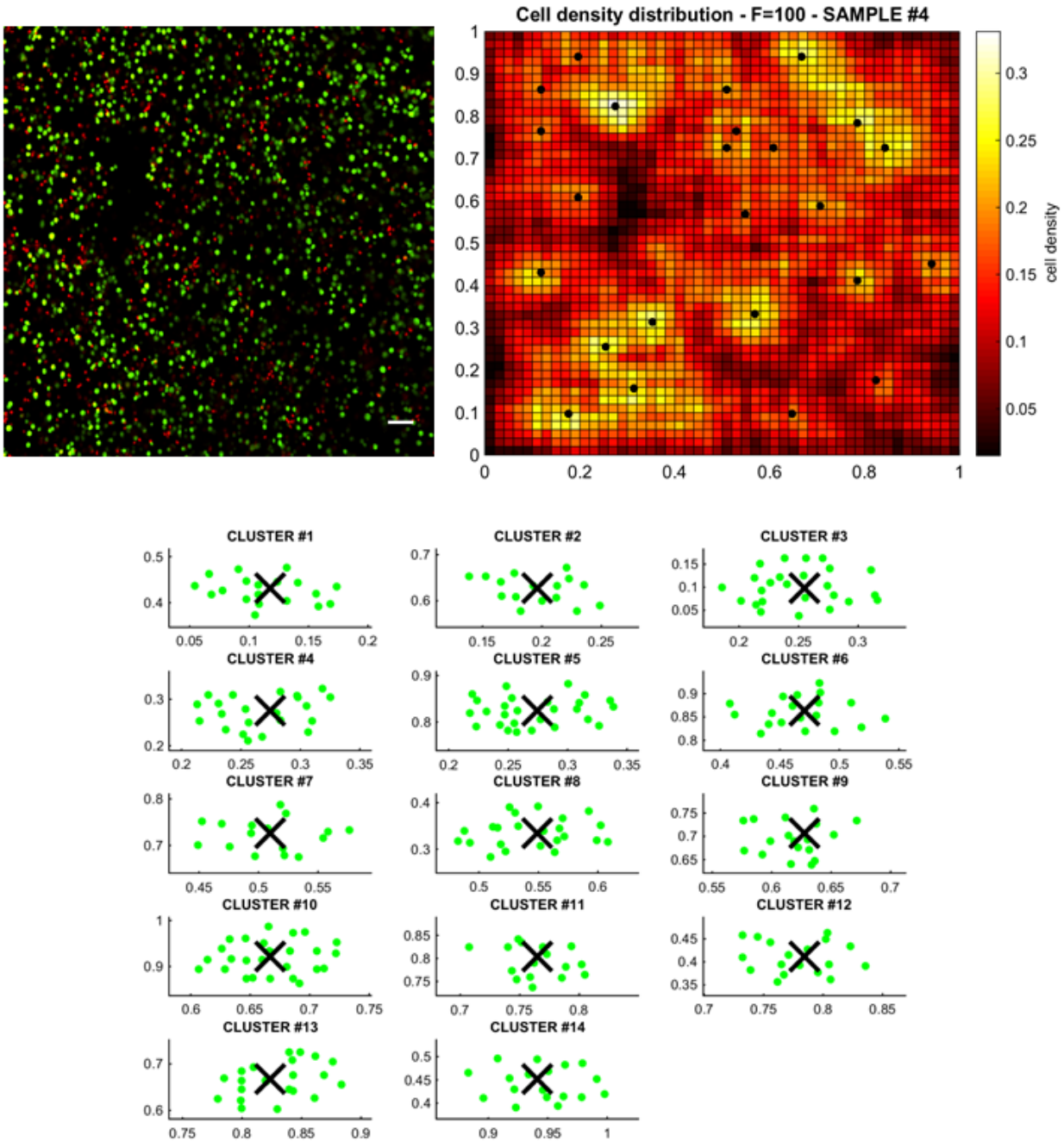

scale. However, in order to process randomly generated data sets they must be interpolated to three dimensional systems.

3.2 Random generation of 3D macroscopic systems

In order to transfer the previous parameters into a three-dimensional system, it is necessary to establish an efficient approach to generalize the data extracted from two-dimensional viability images. It is indicated that a sample represents a slice of 170x170μm^2 for a thickness of 10μm. Therefore the quantity of cells N in the 3D system is obtained by multiplying with the number of slices that must be superposed for a cubic sample:

$$N_{3D} = \frac{L}{\tau} N_{2D} \tag{3.1}$$

where L is the length of the sample (170μm) and τ is its thickness (10μm). In the two dimensional data, the number of clusters and the average cell population of a cluster were also calculated; from which the ratio of cells that are included in a cluster N^* can be deducted. This quantity is assumed to be the same in three dimensions, which results in the following equation:

$$N^*_{3D} = \frac{N^*_{2D}}{N_{2D}} N_{3D} \tag{3.2}$$

This way, it is determined that N^* cells will be allocated in clusters. However, there are still cells that do not belong to any cluster. These single cells are randomly distributed over the entire volume. Since it might intersect with some clusters, it was decided to consider only a given percentage η (90% in the current model) of the cluster population and distribute the rest as single cells in N_{single} to correct the distribution; resulting in the following quantities:

$$N^*_{3D} = \eta \frac{N^*_{2D}}{N_{2D}} \, N_{3D} \quad ; \quad N_{single} = N_{3D} - N^*_{3D} \tag{3.3}$$

Now that the distribution of cells in the clusters is determined, the shape and number of clusters must also be extrapolated in the three dimensional macroscopic system. Clusters are considered to be a multivariate normal distribution of cells. Therefore, they are characterized by two quantities: their mean and their covariance matrix. The mean of each cluster represents its coordinates in the system, and is consequently not important since they will be randomized for system generation. However, the covariance matrix is necessary since it rules the shape and orientation of a cluster. For each cell density, a two-dimensional average covariance matrix V was extracted from the numerical data. It includes the clusters' dimensions on the diagonal terms and their orientation in space on the other terms. Since the orientation is random, we only consider that the eigenvalues of the covariance matrix, a_1 and a_2, are of interest for the analysis. Consequently, only diagonal terms are used to expand this matrix to a 3D model, and the third dimension eigenvalue is expressed as a function of the previous ones: $a_3 = i\ a_1 + j\ a_2$ where i and j are two random quantities included between 0 and 1. To avoid cases of unrealistic flat clusters, i and j cannot be both null at the same time. Therefore, the new covariance matrix can be written as:

$$V = \begin{pmatrix} a_1 & 0 & 0 \\ 0 & a_2 & 0 \\ 0 & 0 & i\ a_1 + j\ a_2 \end{pmatrix} \tag{3.4}$$

Combining the quantities defining the shape of a 3D cluster and the average number of cells in one 2D cluster, the number of cells in a 3D cluster $\overline{N}$ can be evaluated. First, since the values computed in 2D are averaged, they are assumed to be corresponding to the middle section of the cluster, in a slice of 10 μm thickness as shown in figure 3.3. Now, the number of slices required to fill the entire cluster with a rotation around the principal axis must be determined. Since the thickness of one slice as well as the dimensions a_2 and a_3 are known, this quantity can be computed using the perimeter of the ellipse a_2 by a_3 and the thickness of a slice:

Figure 3.3: Three dimensional generalization of cluster distribution - The cluster data derived from experimental images was exploited to create three dimensional systems.

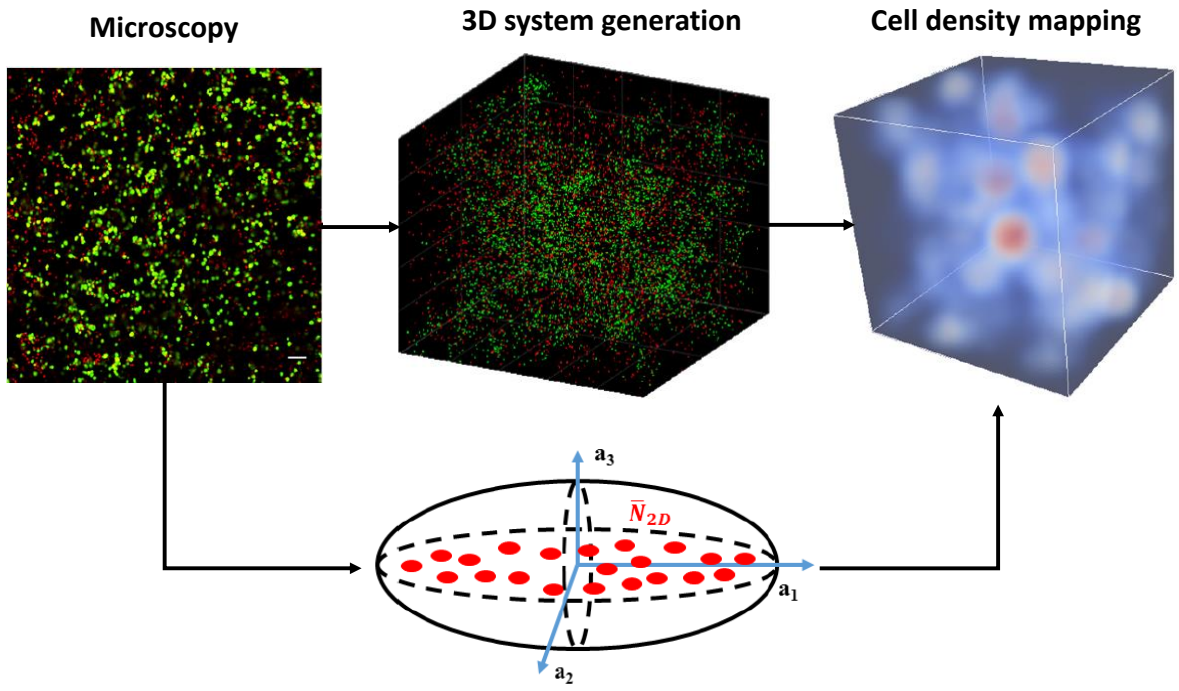

$$\overline{N}_{3D} = \frac{2\pi\sqrt{\frac{a_2^2+a_3^2}{2}}}{2*\tau}\,\overline{N}_{2D} \tag{3.5}$$

Finally, the amount of clusters n for a random 3D distribution for each cell density can be quantified:

$$n_{3D} = \frac{N^*_{3D}}{\overline{N}_{3D}} \tag{3.6}$$

Now, all the necessary quantities to generate a 3D clustered cell distribution have been evaluated to match reality as precisely as possible, as shown in figure 3.3. This way, the model parameters can be matched with experiments to ensure an optimal accuracy in final results. In order to study the influence of cluster distribution parameters on the hydrogel properties, user defined systems with custom cell distributions will be set. By varying the number of clusters n and the density of each cluster a, the performance of each system will be mapped to illustrate the difference between completely homogeneously distributed gels and cluster based heterogeneous cell distribution; which are expected to be more effective for hydrolytically degradable hydrogels. Figure 3.4 illustrates such systems, varying from homogeneous to heterogeneous, and from isolated clusters to a larger cluster distribution.

Figure 3.4: Influence of varying cluster parameters - n gives the number of cluster, and a quantifies the eigenvalues of the covariance matrix characterizing each cluster. That is to say that a small value for a implies compact clusters with a high cell density in the center while a higher value will lead to homogeneous system with very spread clusters.

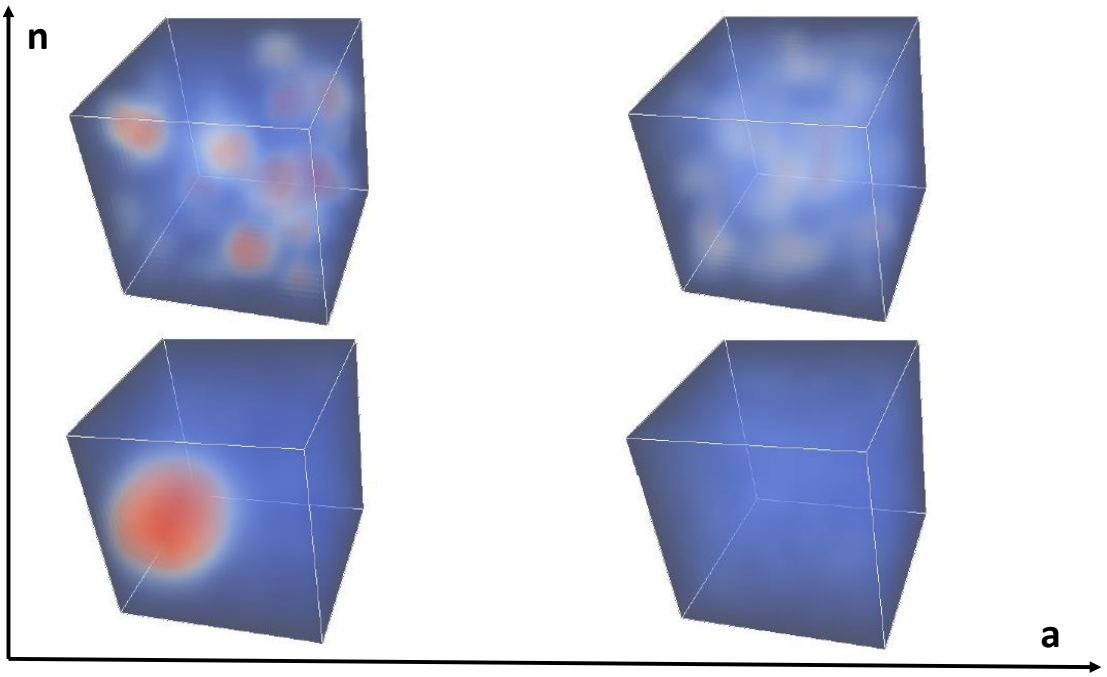

Chapter 4

Results and Interpretations

After completing the model to generate random cell and cluster distributions, it can be used to analyze the evolution of the mechanical properties of different microscopic and macroscopic systems. Several systems will be generated with varying cell density, cell influence radius R_d, and the cluster parameters a and n defined at the end of the previous section. The final objective will be to identify optimal sets of conditions for these parameters in order to obtain a high macroscopic modulus while minimizing its decrease during degradation.

4.1 Influence of cell distribution on a microscopic system

The Young's modulus of material points being unknown in the macroscopic system, it is necessary to study the behavior of microscopic cell distributions prior to clustered systems. To achieve this preliminary objective, a Poisson distribution seemed adapted to generate random cell distributions, making sure that no cells are overlapping, every new system corresponding to a fixed cell density f. For one cell distribution, the polymerization influence ratio R_d is varied from zero to ten times the cell radius, and compared to the average distance between cells $d_{cells}(f)$. This new parameter will be used instead of R_d to determine the optimal influence radius depending on local cell density. For more accuracy, several simulations were ran for each combination of R_d and f.

The microscopic model solves for the degradation and diffusion problems and computes the evolution of the gel modulus in time. Therefore the average cross-linking density and ECM concentration are also computed in time. The results are illustrated in figure 4.1 for a given cell volume

Figure 4.1: Evolution of a microscopic system properties in time - The graphs presented on the left of the figure correspond to simulations for a cell volume fraction $f = 0.2$, a degradation rate $k = 60$, diffusivity $D^* = 0.9$, a deposition rate $\gamma = 0.5$, a critical cross-linking density at reverse gelation $\rho_{critical} = 0.05$ and an ECM stiffness of 40kPa. The simulations which results are shown all have the same microscopic cell distribution, with varying R_d.
The surface on the right side illustrates the mapping of the Young's modulus as a function of cross-linking density and deposited ECM concentration. This surface results from all different combination of f (0.00, 0.05, 0.10, 0.15, 0.20, 0.25, 0.30 and 0.35) and R_d (0, 2, 5 and 10). The surface map was extrapolated from all the simulations, and is not fully covered because the model states that ECM and cross-links cannot coexist at a given material point.

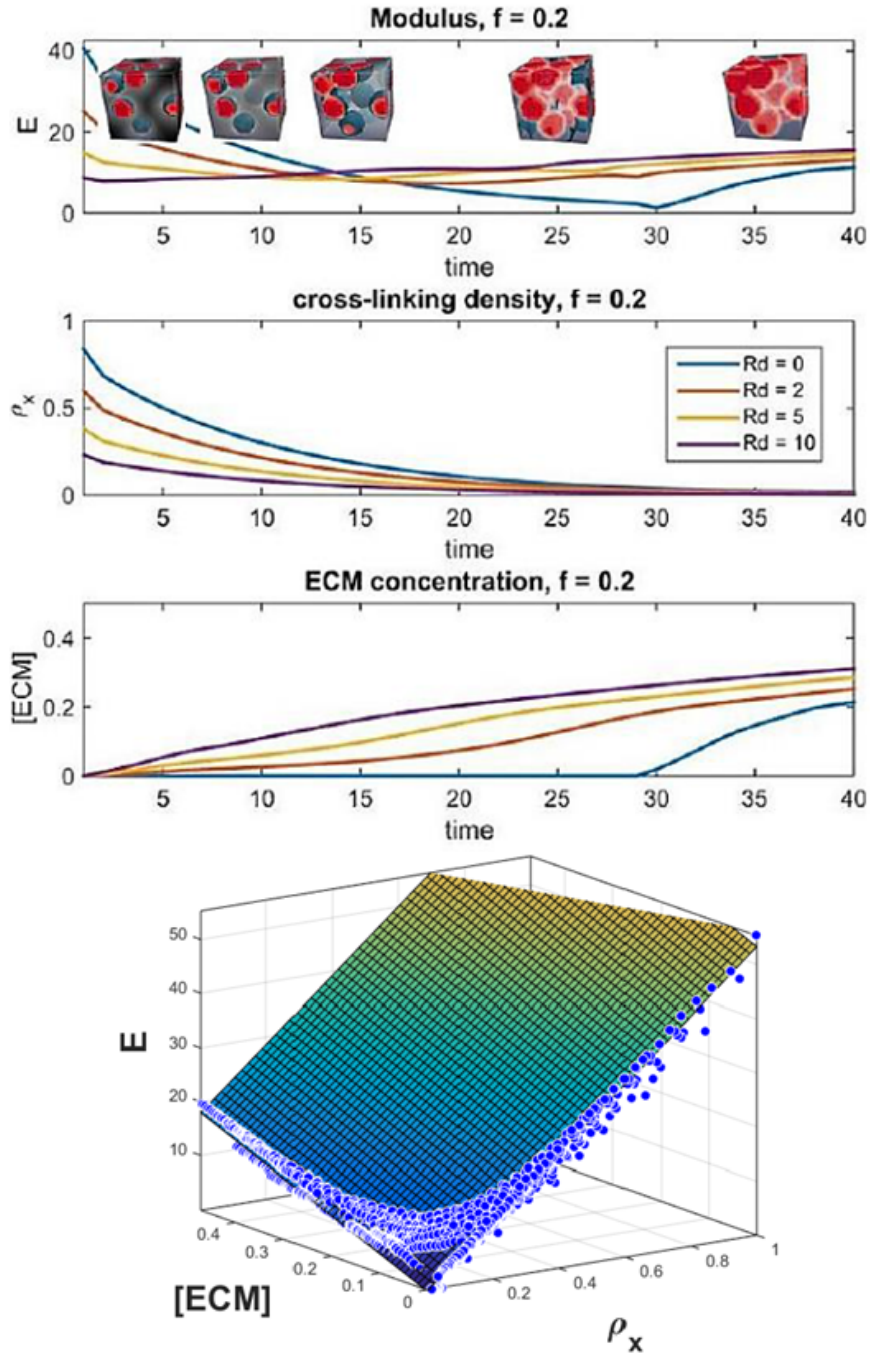

fraction of twenty percent and different values of R_d. The cross-linking density profile follows a first order kinetics equation, and globally decreases when R_d increases. This phenomenon is expected since the influence on polymerization reduces the initial cross-linking density around cells.

Concerning the evolution of the ECM concentration profile, the fact that ECM molecules start to diffuse at a material point only after its reverse gelation has been reached explains the earlier development of new tissue when R_d increases, as well as the stagnation of the system in the case where cross-linking density is not influenced by the cells ($R_d = 0$).

The Young's modulus profile for different values of R_d follows a combination of ECM and cross-linking density profiles with respect to their stiffnesses, which is an expected behavior. On the one hand, the higher R_d is, the lower is the initial modulus due to a low polymerization around cells. On the other hand, the drop in modulus is much smaller because ECM diffusion and deposition are eased by the earlier reverse gelation surrounding cells. However, a quick drop in modulus could be expected due to the influence of R_d when an entire slice of the gel sample loses connectivity before ECM is deposited due to the percolation of regions that reached reverse gelation. Percolation, in this case, is the phenomenon that we observe when regions of reverse gelation connect with each other, and compromise the mechanical integrity of the gel. It was studied using a special case and an unrealistic behavior which only aims to highlight the effect of percolation for degrading areas. A hydrolytically degradable cell seeded system with no ECM production was simulated at the micro-scale. In this simulation, we try to accentuate the potential effect of percolation, which does not appear clearly on the graphs from figure 4.1. To do so, the stiffness of a material point is set to only depend on whether it reached reverse gelation or not. With such a configuration, a quick drop in modulus was indeed observable at the time of percolation. Therefore it can be assumed that the drop in modulus due to the rupture in polymer connectivity is present, but negligible at the micro-scale compared to the constant bulk degradation.

Once the microscopic model is set and enough results have been computed, a relation can be investigated between the modulus of the gel and the initial parameters, as well as with the gel composition (ρ_x and C^*). To begin, a mapping of E, ρ_x and C^* as a function of R_d and f was

established at every time step. Using these maps, it was possible to observe every microscopic result as a combination of average modulus, cross-linking density and ECM concentration. As shown in figure 4.1, all results are situated on the same planar surface, which can lead a simple, bi-linear equation corresponding to:

$$E_{micro} = k_p \rho_x + k_{ECM} C^* \tag{4.1}$$

where k_p represents the polymer stiffness and k_{ECM} the extracellular matrix stiffness. It is important to note that k_{ECM} is unknown, therefore it is also a parameter that can be modified. In this case, it was fixed by the user. The final macroscopic results will be processed for different values of k_{ECM} to investigate its influence. Such a relation implies that using a finite element analysis for microscopic systems is not required anymore. Really, only the degradation and diffusion problems need to be solved and the modulus can be computed from equation (4.1). This equation was also implemented in the macroscopic model to compute the modulus at every point in time. Additionally, it is possible to run many more simulations with bigger ranges for the cell density and R_d parameter, while greatly lowering the computational cost.

4.2 Influence of a clustered distribution on a macroscopic system

Once microscopic simulations have given representative data, the macro-scale model can be implemented with a time dependence. The generation of clustered systems, with an experimental distribution or custom cluster parameters, was established previously. It was seen that a mapping of cell density in the system is necessary to implement a mechanical simulation and compute the evolution of the gel in time.

Using results from the macro-scale the properties of every material point in time can be established from their cell density. First, it is necessary to solve for degradation and diffusion. Since cells are not singled in macroscopic systems, this problem is directly taken from the microscopy.

It is simply done by matching local parameters with f and R_d in the microscopic data, and using the corresponding simulation to obtain the evolution of ρ_x and $[ECM]$ in time. Most microscopic simulations were solved without mechanical loading to save computer power, therefore the modulus is not necessarily known with this method. However, it can be computed using equation (4.1) at every material point. Once the mechanical properties of every material point and their evolution in time are known, a ten percent uni-axial stress in compression is applied, similarly as with the microscopic system. The overall modulus of the gel is then computed through a finite element analysis, using linear elasticity. Results for a macroscopic system with cluster parameters taken from experimental results, a cell density of 150 million cells per milliliter and an R_d of ten times the radius of a cell are shown in figure 4.2. The upper image, showing the system as a cell density mapping illustrates well the apparent cluster distribution, which leads to heterogeneity for the cross-linking degradation, as well as the tissue growth. In this case, the influence of cells on polymerization was set to a high value of R_d. Therefore the initial cross-linking density is low and ECM can diffuse and deposit even during the first time steps. However, even though the modulus does not experience a drop thanks to the fast deposition of new tissue, its initial value remains quite low. This phenomenon lets us assume that there might be combinations of cluster parameters and R_d to reach an optimal evolution in time. The optimal evolution in time is defined by a high initial modulus, and a low drop before tissue growth. It is shown in figure 4.2 that it does not necessarily correspond to a high value of R_d since it lowers quite considerably the initial modulus of the gel.

Macroscopic results can also give a lead to identify the realistic values of R_d parameter by matching initial results from simulations with the experimental initial modulus for each cell density. Such a study is necessary to fully simulate systems close to experiments in the model. Figure 4.3 shows the influence of R_d on the initial modulus. As shown on the figure, the value of R_d matching experimental results varies with the macroscopic cell density. This observation can be explained by the fact that even if R_d quantifies the influence of a single cell on its surrounding cross-links, it does not take into account the fact that cells are closer to each other when their density increases. Therefore the closer the cells are, the bigger the effect of R_d can be expected since the cell influence

Figure 4.2: Evolution of a macroscopic system properties in time

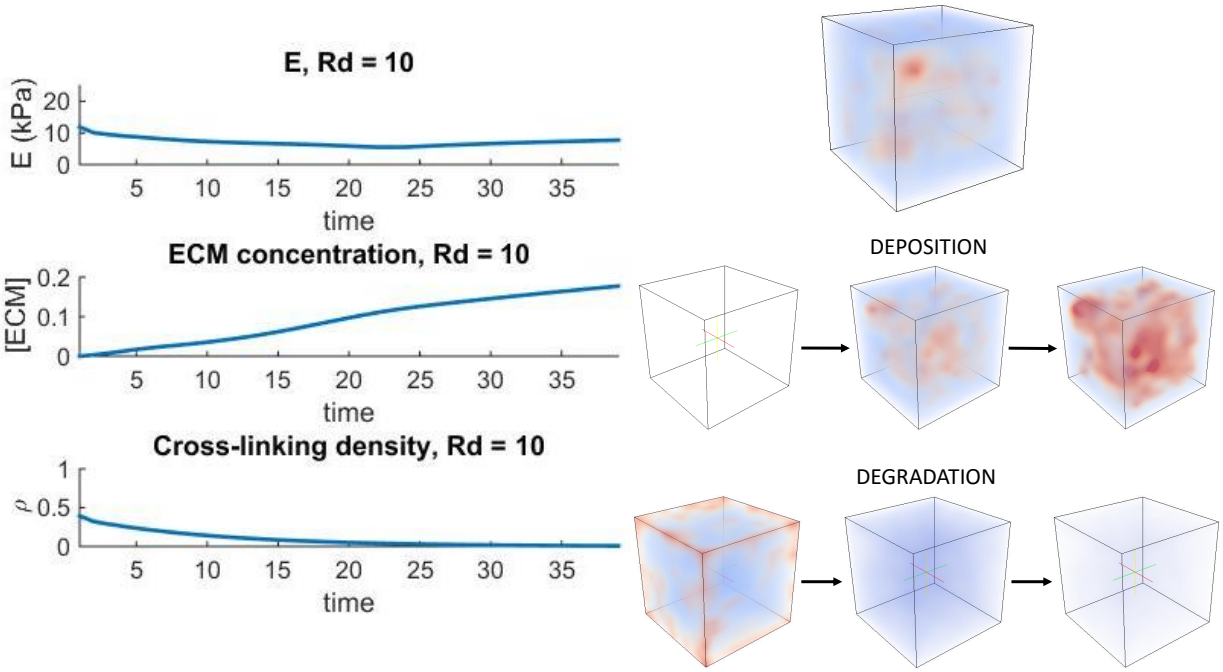

Figure 4.3: Identification of R_d for experimental results

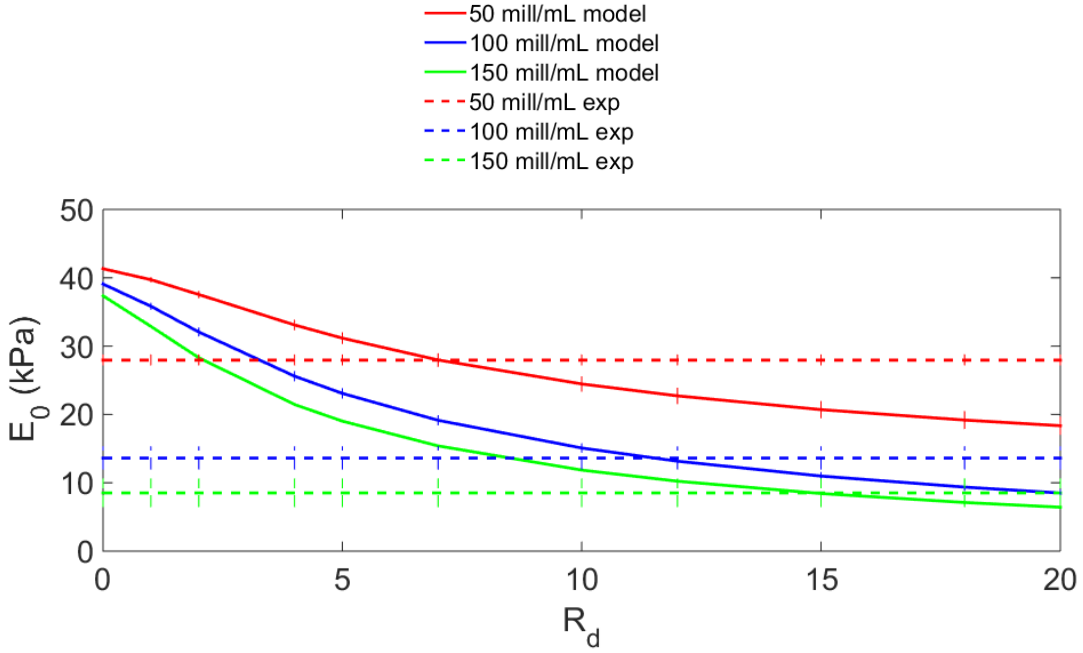

areas will overlap. Consequently, the influence on polymerization might change when there is an overlapping effect.

The overlapping phenomenon of cell influence radius can be evaluated by defining a new parameter d, which relates R_d to the distance between cells for a given cell density at the micro-scale. It is defined by the following equation:

$$d = \frac{2R_d R_{cell}}{d_{cells}} \tag{4.2}$$

where d_{cells} is the average distance between cells for the given cell density. The new d parameter and its influence can easily be illustrated for a microscopic system as shown in figure 4.4. The figure illustrates in detail the influence of R_d on two microscopic systems with different cell volume fractions. The graphs on the left side of the figure expose the average cross-linking density profile between two cells for both systems and different values of R_d, x being the normalized distance between two distinct cell boundaries. They show that for a higher cell density, the overlapping between regions influenced by cells will differ, leading to different cross-linking densities even though the value of R_d is constant. Finally, the right part of the figure illustrates the effect of both R_d and d on the initial modulus. The results are plotted as the ratio of E_0 for a positive value of R_d over E_0 for an R_d of zero, corresponding to the case where cells have no influence on polymerization. It exhibits that for the same value of R_d, the modulus decreases considerably more for a high cell density system. On the opposite, the initial modulus seem to follow the same profile with respect to d for both cell densities. It seems to explain the variation between macroscopic systems, for which R_d will have a greater influence at high cell densisties. However local cell density greatly varies inside a macroscopic systems, and a global d parameter cannot be precisely defined for such systems even though it seems to explain the previous observations.

Such results seem to confirm the hypothesis established earlier, which supposed that cells have a considerable effect on polymerization, leading to lower initial modulus and better growth

Figure 4.4: Influence of d parameter on microscopic systems

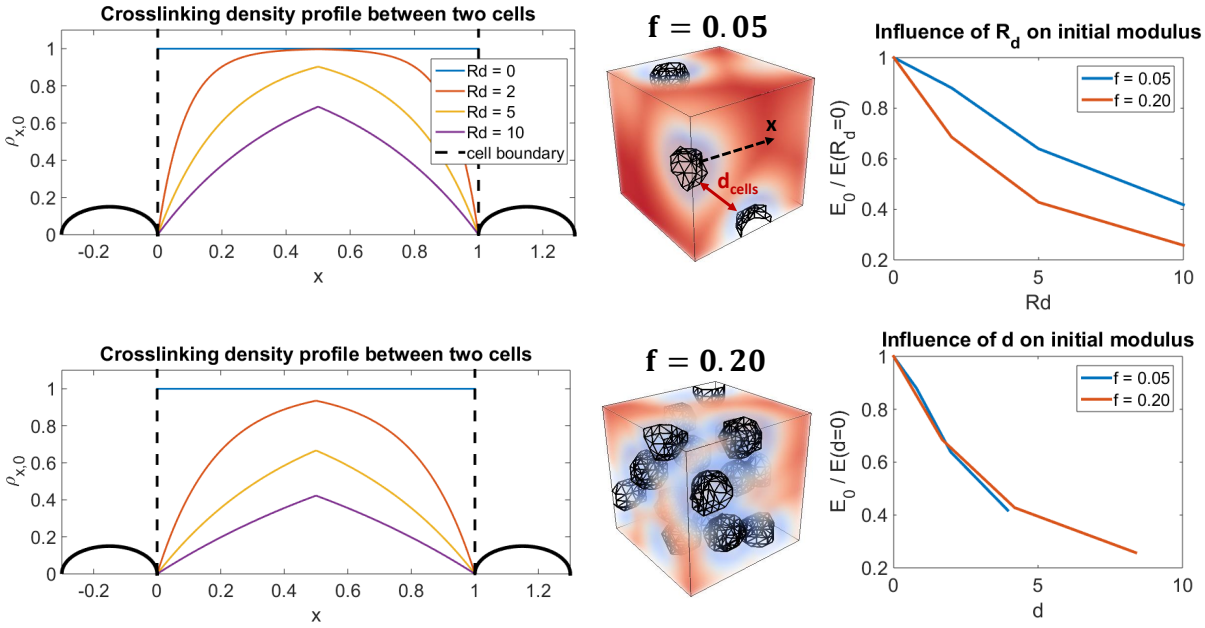

for a hydrolytically degradable hydrogel. However, the hypothesis that cell distribution, especially in clustered systems, greatly influences the viability of a cell-seeded hydrogel and its mechanical properties remains to be confirmed.

4.3 Final results and effect of cluster parameters on mechanical properties

In order to study the influence of cluster parameters for a given combination of R_d and macroscopic cell density F, several simulations were ran with user defined cell distributions. For each simulation, three results are considered to evaluate the viability. They are illustrated in figure 4.3. The initial modulus must be high enough to support mechanical loads at early time steps and during the degradation phase, the drop in modulus must be minimized and the ending modulus must be maximized. These quantities must be compared to a critical value of the modulus, at which the integrity of the gel is compromised and its load-bearing capacity is too weak. Therefore, an optimized system will simply be defined as a system for which the modulus always remains above the $E_{critical}$ value. For several combinations of macroscopic cell density, R_d parameter and ECM stiffness, the minimum and maximum moduli were mapped as a function of cluster distribution parameters a and n. As defined previously in section 3.2, n represents the number of clusters is the system, and a is the average eigenvalue of the cluster covariance matrix. That is to say that clusters are very spread and homogeneous when a is large, or small and dense when it is smaller as illustrated in three dimensions in figure 3.4. Figure 4.6 illustrates such results for a specific combination, and aims to observe which cell distributions are best to optimize tissue growth and the mechanical properties of the medium over time by crossing the different diagrams of the resulting figure. The effects of varying cluster parameters on initial cell density and ECM deposition are also illustrated for different systems. For clarity purposes, figure 4.6 only displays results for a given combination of design parameters, several simulations were ran for F=50, 100 and 150 million cells per mL, R_d=0, 2, 5 and 10 times the cell radius (from cell boundary) and k_{ECM}=40 and 100. Therefore results such as tables C.1 and C.2 can easily be computed by the model for various simulations, and might result in slighlty different optimal cluster parameters. Additionally, the model can be

Figure 4.5: Quantities used to evaluate the efficiency of a cell distribution

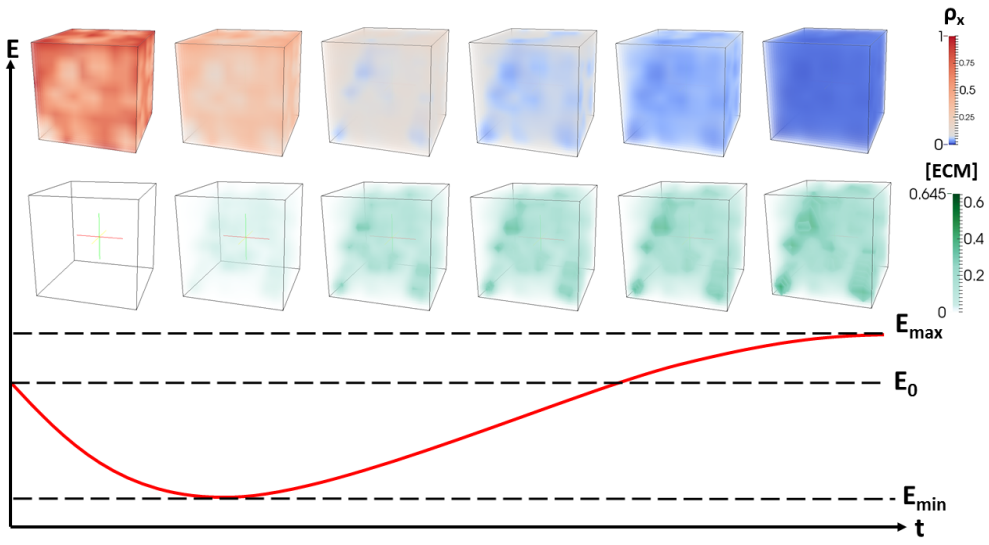

Figure 4.6: Mapping of minimum and maximum modulus as a function of cluster distribution parameters for a user defined combination of macroscopic cell density, R_d and ECM stiffness. A red region is set, representing combinations leading to a modulus lower than the critical value of 10 kPa.

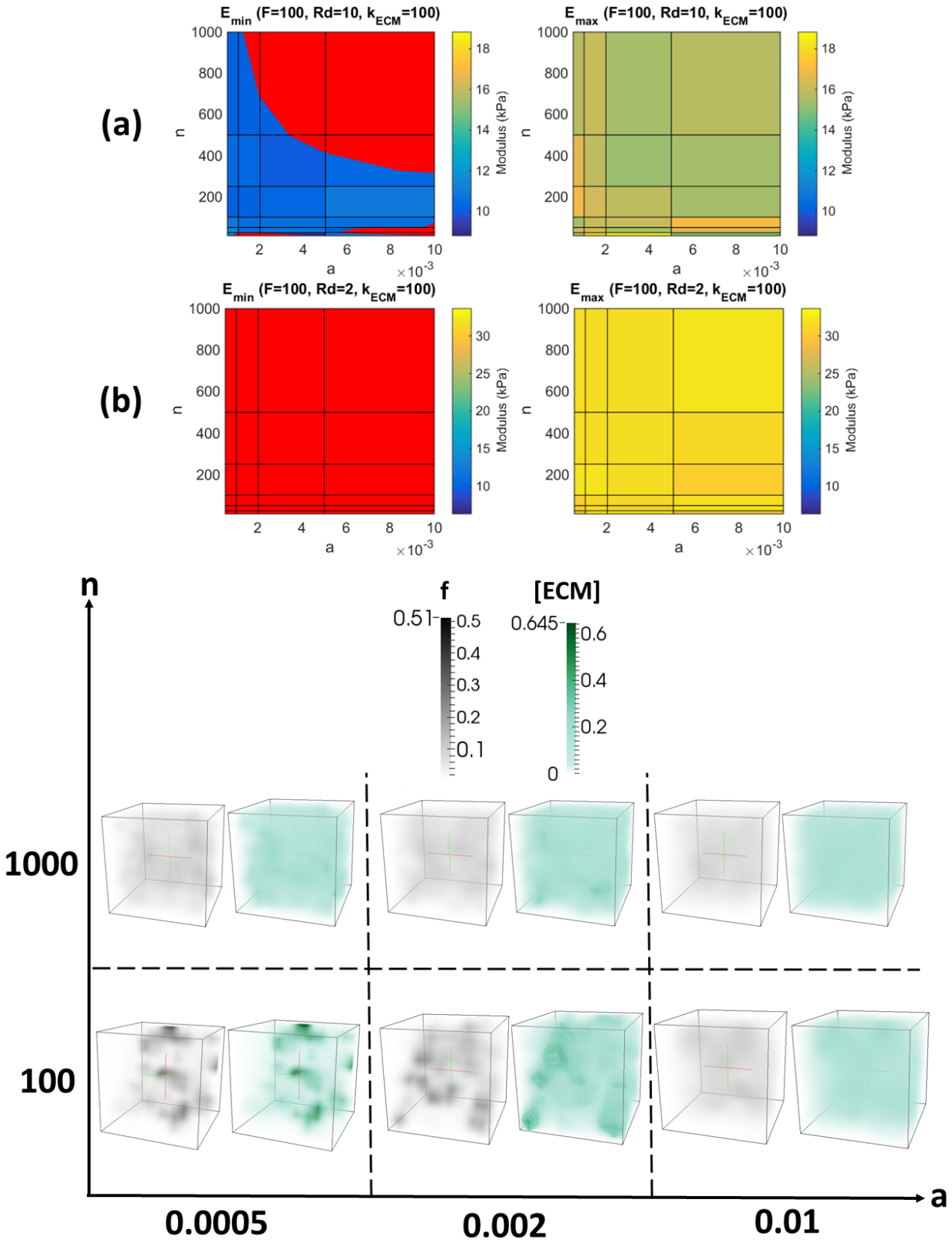

used to cover bigger ranges for n, a and k_{ECM} parameters set by the user.

On figure 4.6, it is possible to observe an expected behavior from the gel, as well as the influence of the cell influence parameter R_d. Figure 4.6-(a) shows a red area on the minimum modulus diagram. The red area underlines all cluster parameter combinations which lead to a modulus below the critical value of 10 kPa during the growth process. In that event, the corresponding cluster distribution of cells is not viable since it provokes a drop in modulus too important to bear physiological loads at all times during growth. Now, by focusing on the coordinates of such combinations, it appears that such regions range from a high number of very dense clusters to a medium number of highly spread clusters. In the case of numerous dense clusters, the distribution approaches a case of single cells spread around the entire gel, which is almost equivalent to a homogeneous distribution. Similarly, a large quantity of clusters that have a low density (which implies that the cluster population are spread in space) will lead to a system close to a homogeneous distribution since clusters intersect with each other. Consequently, it seems that homogeneous distribution are not conclusive in this case. On the countary, regions below that line will have clustered heterogeneous distributions as described earlier, and keep a reasonably strong modulus at the critical stage of growth between the end of degradation and the beginning of ECM tissue connectivity. For clarity purposes, the scale is set to be the same for the minimum and maximum modulus diagram. As a consequence, the minimum modulus diagram seems uniform as all valus are in a close range between 10kPa and 12kPa. However it is not the case as shown in the results presented in appendix C.

Furthermore, figure 4.6-(b) exposes the same combinations, for a weaker influence of cells on polymerization. In this case, ECM can only diffuse close to the chondrocytes which leads to a slower deposition of connected tissue compared to the degradation process. Such initial conditions might seem beneficial, reducing the infuence of cells on polymerization to ensure a high initial modulus, but still allowing diffusion before the gel degrades completely. However, it is easily observable that there is not enough growth before the gel reaches reverse gelation leading to a clear modulus drops at the critical point of degradation. This phenomenon demonstrate this importance of both diagrams on the figure: higher values for maximum modulus might not necessary be beneficial.

The diagrams must be combined to avoid dropping the modulus below the critical value while maximising the modulus of the gel during tissue growth.

Chapter 5

Conclusion

As a summary, we introduced a model which aims to investigate the conditions favorable to tissue growth in hydrolytically degradable hydrogels, and give possible solutions for such a problem. This intention came from the observations in experimental results that successful results seem to vary for hydrogels with bulk degradation. Consequently, obtaining quantitative data from a numerical model could help significantly in the search of possible explanations. Two important hypothesis were assumed based on experiments and represent a keystone of the model. The first one, based on measurements of initial modulus while changing the cell concentration, stated that cells have an influence on polymerization during the synthesis of a cell-seeded hydrogel. Therefore, regions of low cross-linking density are supposed to be present around chondrocytes, which facilitates the early diffusion of ECM molecules prior to complete degradation of the medium. From the first hypothesis, the second assumption we made supposed that since growth can happen surrounding cells at early time steps, the cell distribution might be a key parameter to understand the behavior of hydrolytically degradable gels. This model presents interesting features because it emphasizes the fact that having heterogeneity in cell distributions could be beneficial to achieve successful growth.

The influence of cells on the initial cross-linking density profile was implemented in the model by introducing an influence radius parameter R_d, expressed as a function of the cell radius. Then, a function was built to express the evolution of cross-links around the cells as a diffusion profile based on experimental observations. Once clearly defined, the polymer network degradation and

ECM diffusion/deposition could be implemented with a simple finite difference method, following first order kinetics and Fick's laws of diffusion. Finally, the evolution of a hydrogel with a user defined density of encapsulated cells was simulated at the microscopic scale. Cells are randomly distributed following a Poisson distribution, and their influence on the local cross-linking density was implemented. However, the chemical composition of the system is not enough to derive its mechanical properties; thus the necessity for a finite element method computing the modulus of the gel over time. In this model, a simple linear elastic approach was used to simplify the problem, which in our case focuses on cell distribution and influence more than that of material properties. However, improvements could be applied in later projects to improve the mechanical model used in the current state. The simulations resulted in tables mapping the evolution of Young's modulus in microscopic volumes as a function of cross-linking density, and the influence of R_d on the mechanical performance and tissue growth in time.

In the interest of modelling macroscopic systems from the new data, we analyzed cell distribution in experimental samples to set parameters ruling the level of heterogeneity in the system. From this analysis, two types of simulations were used: realistic and user defined. Realistic simulations simply used a cell distribution similar to the one observed in experimental samples. User defined simulations are based on the distribution parameter definitions extracted from experimental sample, but their values are set by the user. In macroscopic systems, each material point corresponds to a distinct microscopic system with its own cell density. Therefore their time dependant properties can be extracted from microscopic data, and a homogenization process is used to obtain the evolution of a macroscopic system over time.

From the final results, tables and diagrams were created to illustrate the viability of a system based on its initial state (cell density, cell influence radius, cluster parameters). The tendency seems to encourage our main hypothesis that heterogeneity helps creating a connected network of deposited ECM resulting in successful tissue growth. To conclude, it can be noted that these diagrams and tables can bring assistance to experimentalists. The model could be used to predict or optimize the behavior of hydrolytically degradable hydrogels in which they encapsulate stem cells to

trigger the growth of biological tissues. Additionally, in view of a patient based procedure, a model such as the one developed in this thesis could be interesting. Using a large database of optimal conditions for a given combination of cell distribution, a personalized gel could be investigated by studying the patient's cells and finding the design parameters necessary to produce an efficient hydrogel.

Bibliography

[1] C. G. Armstrong and V. C. Mow. Variations in the intrinsic mechanical properties of human articular cartilage with age, degeneration, and water content. J Bone Joint Surg Am, 64(1):88–94, January 1982.

[2] Azita Belashi. Percolation Modeling in Polymer Nanocomposites. PhD thesis, University of Toledo, 2011.

[3] Stephanie J. Bryant and Kristi S. Anseth. Hydrogel properties influence ECM production by chondrocytes photoencapsulated in poly(ethylene glycol) hydrogels. Journal of Biomedical Materials Research, 59(1):63–72, January 2002.

[4] Valentin Dhote, Stacey Skaalure, Umut Akalp, Justine Roberts, Stephanie J. Bryant, and Franck J. Vernerey. On the role of hydrogel structure and degradation in controlling the transport of cell-secreted matrix molecules for engineered cartilage. Journal of the Mechanical Behavior of Biomedical Materials, 19:61–74, March 2013.

[5] Valentin Dhote and Franck J. Vernerey. Mathematical model of the role of degradation on matrix development in hydrogel scaffold. Biomechanics and modeling in mechanobiology, 13(1), January 2014.

[6] Michael A. DiMicco and Robert L. Sah. Dependence of Cartilage Matrix Composition on Biosynthesis, Diffusion, and Reaction. Transport in Porous Media, 50(1-2):57–73.

[7] P. A. Durbin and G. Iaccarino. An Approach to Local Refinement of Structured Grids. J. Comput. Phys., 181(2):639–653, September 2002.

[8] I. Farmaga, M. Lobur, P. Shmigelskyi, N. Javorskyi, and P. Spiewak. Regular and adaptive meshing algorithms for modeling of spherical inclusions by finite element method. In 2012 International Conference on Modern Problems of Radio Engineering Telecommunications and Computer Science (TCSET), pages 505–507, February 2012.

[9] F. Guilak, W. R. Jones, H. P. Ting-Beall, and G. M. Lee. The deformation behavior and mechanical properties of chondrocytes in articular cartilage. Osteoarthritis and cartilage / OARS, Osteoarthritis Research Society, 7(1):59–70, January 1999.

[10] Mansoor A. Haider, Jeffrey E. Olander, Rachel F. Arnold, Daniel R. Marous, April J. McLamb, Karmethia C. Thompson, William R. Woodruff, and Janine M. Haugh. A phenomenological mixture model for biosynthesis and linking of cartilage extracellular matrix in scaffolds seeded with chondrocytes. Biomechanics and Modeling in Mechanobiology, 10(6):915–924, December 2011.

[11] Pierre-Yves Hicher and Ching S. Chang. A Multiscale Modeling of Granular Materials with Surface Energy Forces. In Oana Cazacu, editor, Multiscale Modeling of Heterogenous Materials, pages 293–317. ISTE, London, UK, January 2008.

[12] T. A. Holland, E. W. H. Bodde, V. M. J. I. Cuijpers, L. S. Baggett, Y. Tabata, A. G. Mikos, and J. A. Jansen. Degradable hydrogel scaffolds for in vivo delivery of single and dual growth factors in cartilage repair. Osteoarthritis and cartilage / OARS, Osteoarthritis Research Society, 15(2):187–197, February 2007.

[13] Dietmar W. Hutmacher, Michael Sittinger, and Makarand V. Risbud. Scaffold-based tissue engineering: rationale for computer-aided design and solid free-form fabrication systems. Trends in Biotechnology, 22(7):354–362, July 2004.

[14] Yoshito Ikada. Challenges in tissue engineering. Journal of the Royal Society Interface, 3(10):589–601, October 2006.

[15] Shengmao Lin and Linxia Gu. Influence of Crosslink Density and Stiffness on Mechanical Properties of Type I Collagen Gel. Mechanical & Materials Engineering Faculty Publications, January 2015.

[16] N. Lombardo and N. Lombardo. Properties of composites containing spherical inclusions surrounded by an inhomogeneous interphase region. 2007.

[17] J. Pablo Marquez, Guy M. Genin, Kenneth M. Pryse, and Elliot L. Elson. Cellular and matrix contributions to tissue construct stiffness increase with cellular concentration. Annals of Biomedical Engineering, 34(9):1475–1482, September 2006.

[18] Andrew T. Metters, Christopher N. Bowman, and Kristi S. Anseth. A Statistical Kinetic Model for the Bulk Degradation of PLA-b-PEG-b-PLA Hydrogel Networks. The Journal of Physical Chemistry B, 104(30):7043–7049, August 2000.

[19] Ryan James Monroe. Measuring the Mechanical Response of Swollen Hydrogels. ProQuest, 2008. Google-Books-ID: 1Pf8MIUVFE4C.

[20] Garret D. Nicodemus and Stephanie J. Bryant. Cell Encapsulation in Biodegradable Hydrogels for Tissue Engineering Applications. Tissue Engineering Part B: Reviews, 14(2):149–165, June 2008.

[21] Stacey C. Skaalure, Umut Akalp, Franck J. Vernerey, and Stephanie J. Bryant. Tuning Reaction and Diffusion Mediated Degradation of Enzyme-Sensitive Hydrogels. Advanced Healthcare Materials, 5(4):432–438, February 2016.

[22] H. Tan, Y. Huang, C. Liu, and P. H. Geubelle. The MoriTanaka method for composite materials with nonlinear interface debonding. International Journal of Plasticity, 21(10):1890–1918, October 2005.

[23] Tim Topoleski. Atherosclerotic Lesions: Mechanical Properties. In Peter Lanzer MD and Eric J. Topol MD, editors, Pan Vascular Medicine, pages 340–352. Springer Berlin Heidelberg, 2002. DOI: 10.1007/978-3-642-56225-9_21.

[24] Salvatore Torquato. Random Heterogeneous Materials: Microstructure and Macroscopic Properties. Springer Science & Business Media, April 2013.

[25] Franck J. Vernerey. A mixture approach to investigate interstitial growth in engineering scaffolds. Biomechanics and Modeling in Mechanobiology, 15(2):259–278, April 2016.

[26] I. Villanueva, D.S. Hauschulz, D. Mejic, and S.J. Bryant. Static and dynamic compressive strains influence nitric oxide production and chondrocyte bioactivity when encapsulated in PEG hydrogels of different crosslinking densities. Osteoarthritis and Cartilage, 16(8):909–918, August 2008.

[27] J. H.-C. Wang and B. P. Thampatty. An introductory review of cell mechanobiology. Biomechanics and Modeling in Mechanobiology, 5(1):1–16, March 2006.

Appendix A

Cluster distribution parameters extracted from experimental image analysis

Table A shows the numerical values of the cluster parameters previously listed in chapter 3, and figures A.1, A.2 and A.3 illustrate the experimental microscopy images from which they were extracted. The average covariance matrix are 2x2 symmetric diagonal matrices, therefore only the diagonal term is shown in the tables.

Table A.1: Cell distribution parameter extracted from microscopy images - Distance parameters were computed for a sample with normalized dimensions of 1x1

50mill/mL	n_{cells}	$n_{clusters}$	spacing	radius	covariance	$density_{max}$	noise
	491	25	0.14	0.051	0.0015	0.08	146
100mill/mL	n_{cells}	$n_{clusters}$	spacing	radius	covariance	$density_{max}$	noise
	910	22	0.15	0.057	0.0019	0.14	307
150mill/mL	n_{cells}	$n_{clusters}$	spacing	radius	covariance	$density_{max}$	noise
	782	21	0.15	0.057	0.0019	0.12	279

Figure A.1: Microscopy images for a cell density of 50 million cells/mL

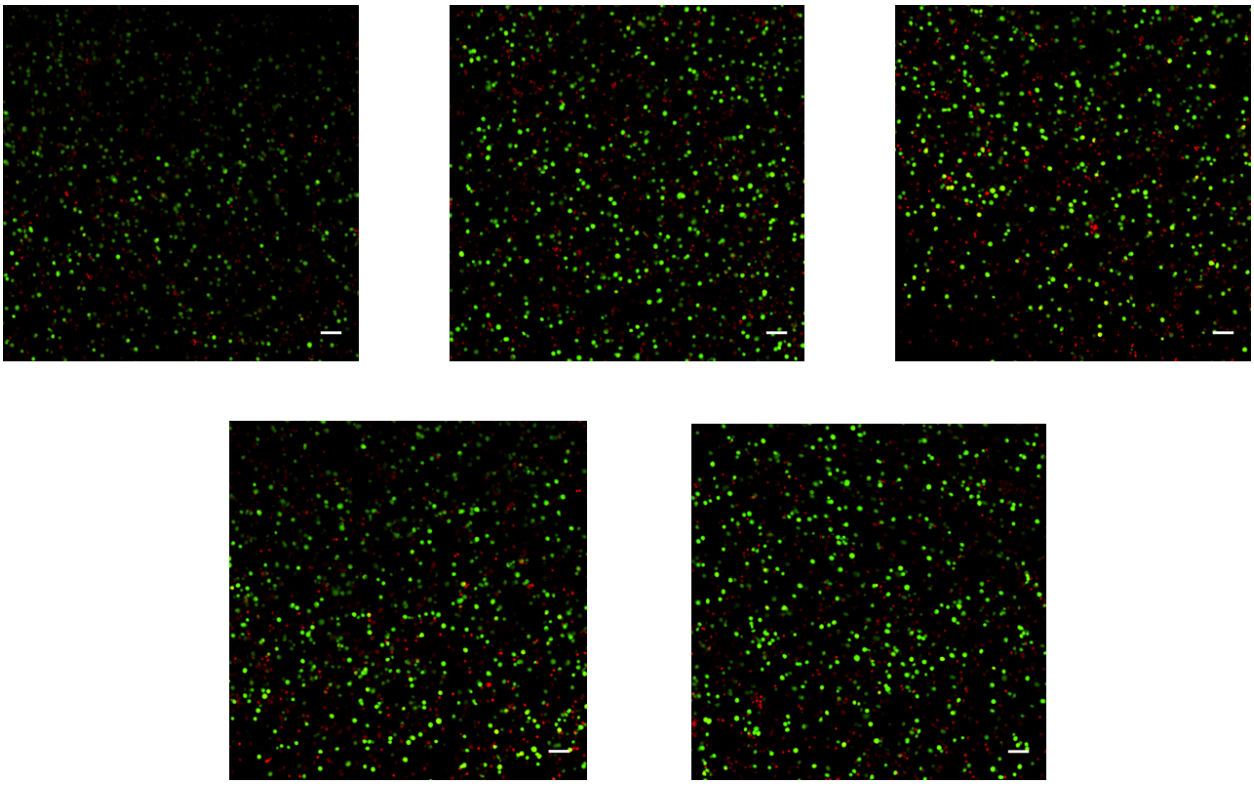

Figure A.2: Microscopy images for a cell density of 100 million cells/mL

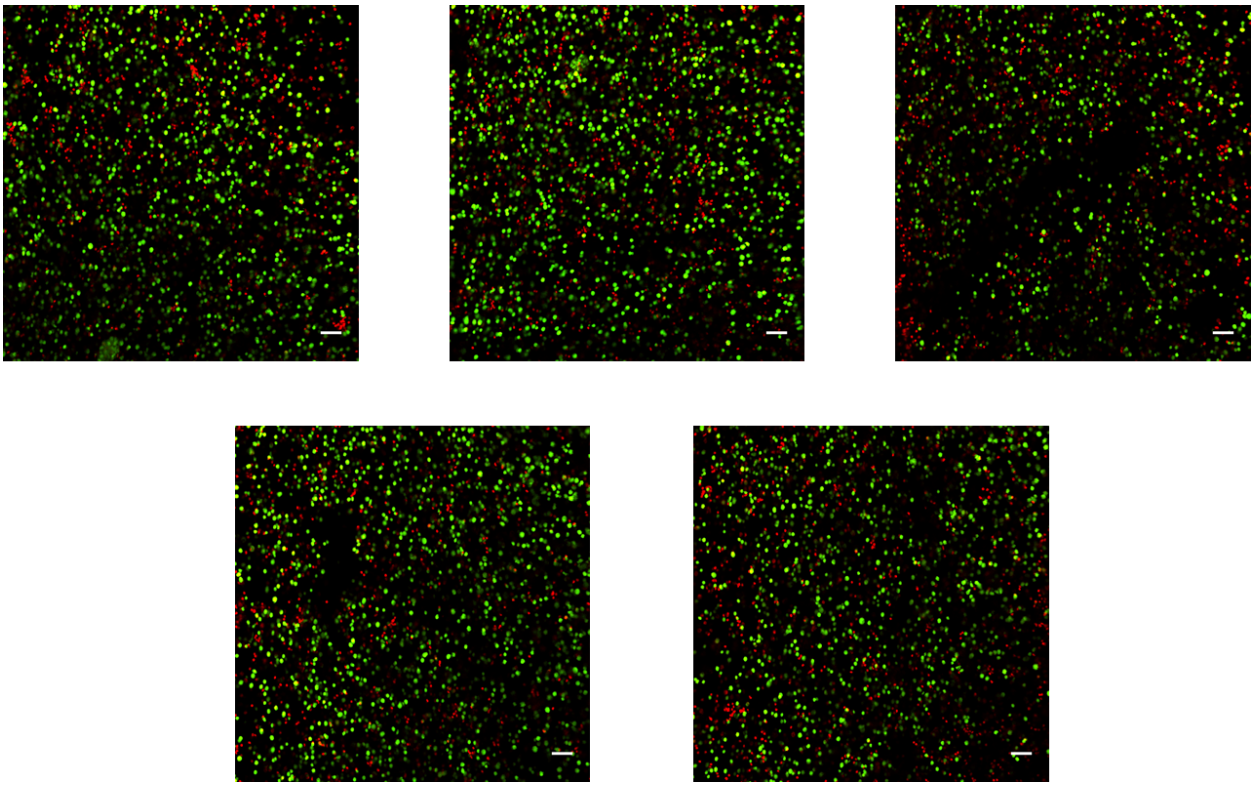

Figure A.3: Microscopy images for a cell density of 150 million cells/mL

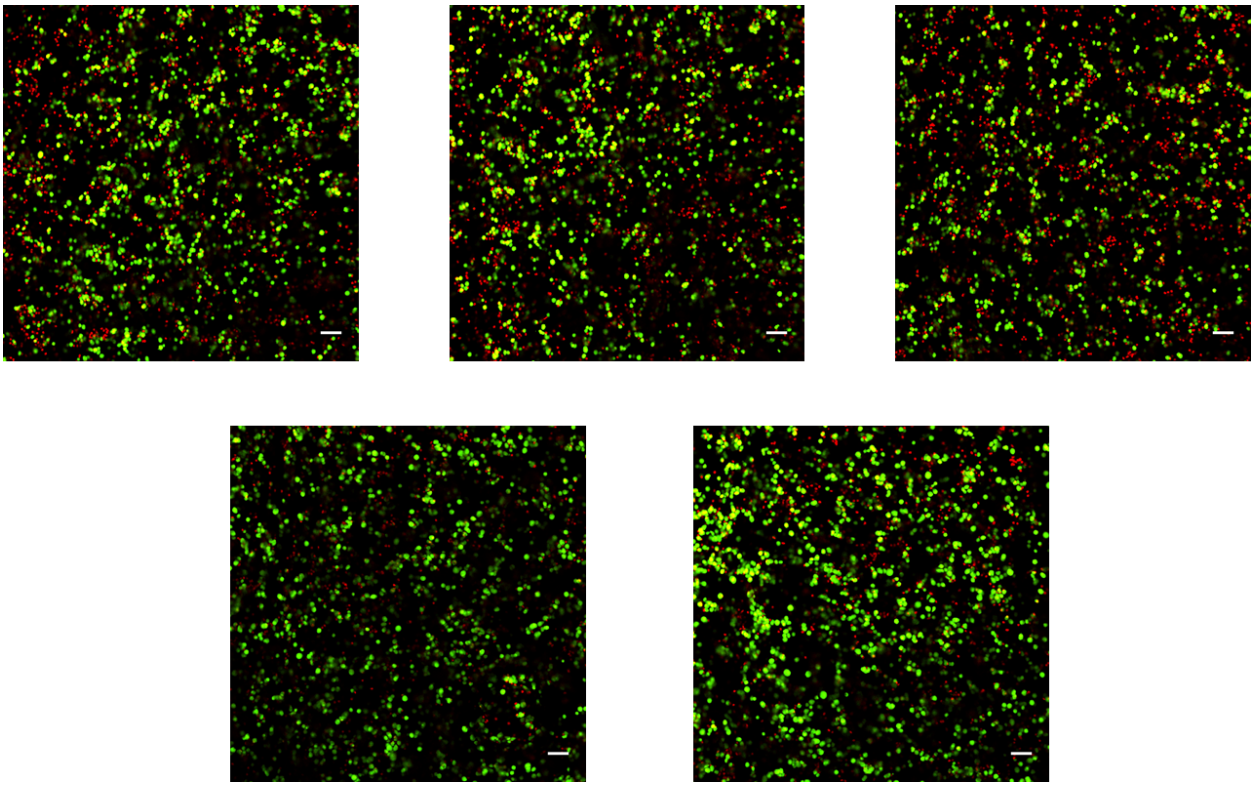

Appendix B

Equivalence between R_d and d parameter

The table B exhibited in this appendix shows the relation between the parameters d, R_d and f. d is important to evaluate the cross-linking density profile at the micro-scale, as it takes into account the average distance between cells. However, this parameter does not transfer to macroscopic heterogeneous systems since the local cell density differs considerably within the system. Consequently, it is not possible to obtain a characteristic value of d at the macro-scale.

Table B.1: Values of d parameter for various combinations of R_d and microscopic cell densities

Rd \f	0	0.03	0.05	0.1	0.15	0.2	0.25	0.3	0.35
1	0	0.35	0.54	0.7	0.79	0.84	0.87	0.89	0.91
2	0	0.7	1.09	1.4	1.57	1.68	1.73	1.79	1.82
4	0	1.41	2.18	2.8	3.15	3.36	3.46	3.58	3.63
5	0	1.76	2.72	3.5	3.93	4.2	4.33	4.47	4.54
7	0	2.47	3.81	4.91	5.5	5.88	6.06	6.26	6.35
10	0	3.52	5.44	7.01	7.86	8.4	8.65	8.94	9.08
12	0	4.23	6.53	8.41	9.44	10.08	10.39	10.73	10.89
15	0	5.29	8.16	10.51	11.8	12.6	12.98	13.41	13.62
18	0	6.34	9.79	12.62	14.15	15.12	15.58	16.1	16.34

Appendix C

Numerical values of the influence of cluster distribution parameters

Tables C and C shows the numerical values illustrated in figure 4.6. These results aim to help experimentalists in the design of viable cell-seeded hydrogels submitted to hydrolytic degradation.

Table C.1: Influence of cluster parameters on minimum modulus

Rd 10	n \a	0.0005	0.001	0.002	0.005	0.01
	10	11.42	9.43	9.03	11.03	10.95
	25	11.40	10.62	10.76	10.21	8.81
	50	10.85	10.59	10.63	10.58	9.94
	100	10.19	10.15	10.24	10.90	10.09
	250	10.48	10.25	10.01	10.26	10.06
	500	10.10	10.18	10.11	9.87	9.84
	1000	10.23	10.06	9.83	9.94	9.82
Rd 2	n \a	0.0005	0.001	0.002	0.005	0.01
	10	7.50	6.65	6.57	7.54	7.79
	25	7.51	7.14	7.31	6.95	6.36
	50	7.34	7.14	7.13	7.06	6.73
	100	6.88	6.94	7.02	7.38	7.19
	250	7.05	7.02	6.95	7.07	6.91
	500	6.95	6.96	6.99	6.84	6.82
	1000	7.09	6.90	6.79	6.82	6.78

Table C.2: Influence of cluster parameters on maximum modulus

Rd 10	n \a	0.0005	0.001	0.002	0.005	0.01
	10	15.84	17.94	18.82	15.06	16.94
	25	16.24	16.27	15.45	16.51	17.79
	50	15.41	16.09	16.12	17.09	18.43
	100	16.94	16.30	15.91	15.53	14.38
	250	16.49	15.97	15.34	15.44	16.08
	500	15.75	16.04	15.43	15.84	15.92
	1000	15.01	16.09	16.16	16.35	16.20
Rd 2	n \a	0.0005	0.001	0.002	0.005	0.01
	10	30.31	32.89	33.12	30.19	28.76
	25	30.37	31.53	30.82	32.01	33.63
	50	30.64	31.37	31.34	31.70	32.82
	100	32.18	31.97	31.67	30.62	30.79
	250	31.63	31.66	31.72	31.40	31.93
	500	31.76	31.80	31.60	32.08	32.14
	1000	31.24	31.96	32.27	32.20	32.27